Silent reservoirs are shaping disease emergence: the case of Usutu virus in the Netherlands

M.M. de Wit[1], G. Beaunée[2]*, M. Dellar[3, 4]*, E. Münger[5*], L. Krol[3], N. Atama[5], J. van Irsel[6,7], H. van der Jeugd[6], M. Koopmans[5], M.C.M. de Jong[1], R. S. Sikkema[5], Q. ten Bosch[1]

* Authors contributed equally

1. Infectious Disease Epidemiology, Department of Animal Sciences, Wageningen University and Research, Wageningen, the Netherlands
2. Oniris, INRAE, BIOEPAR, 44300, Nantes, France
3. Institute of Environmental Sciences, University of Leiden, Leiden, The Netherlands
4. Deltares, Utrecht, The Netherlands
5. Viroscience, Erasmus MC, Rotterdam, Netherlands
6. Vogeltrekstation- Dutch Centre for Avian Migration and Demography, Netherlands Institute of Ecology NIOO-KNAW, Wageningen, The Netherlands
7. Radboud Institute for Biology and Environmental Sciences, Radboud University, Nijmegen, The Netherlands

Corresponding author: Mariken de Wit
Email: mariken.dewit@wur.nl
Classification: Biological Sciences – Ecology
Keywords: mosquito-borne diseases, mathematical modelling, Usutu virus, multi-host disease

Abstract

Disentangling contributions of different hosts to disease emergence and spread is highly complex, but critical for improving predictions, surveillance, and response. This is particularly challenging in wildlife, with pathogens often infecting multiple species and data collection being difficult. Using the emergence of Usutu virus (USUV) in the Netherlands as a case study, we demonstrate the use of an Approximate Bayesian Computation framework on diverse data sources to uncover hidden drivers of spatio-temporal wildlife disease emergence. We calibrated single- and multi-host mechanistic transmission models to five types of wildlife surveillance and research data, describing molecular and serological evidence of USUV in wild birds. Although Eurasian blackbirds, the primary sentinel species, were the most severely affected species, our models indicated that USUV could not persist in blackbirds alone. Our data-model framework provided statistical support for additional bird species to have contributed to transmission. This population of bird species is characterised by limited infection mortality, a longer lifespan, and likely further dispersal than blackbirds. Immunity in this reservoir population appears to have protected blackbirds from further USUV-related population decline. Continued surveillance could help identify these reservoir species. Our results underscore the importance of considering multiple host populations to understand outbreak dynamics. Neglecting the multi-host context of disease transmission can impact the reliability of future predictions and the projected impact of intervention strategies.

Significance statement

Understanding which species contribute to disease transmission is critical for improving predictions, surveillance, and response. However, disentangling these contributions is difficult, especially for wildlife diseases where pathogens often infect multiple species and data collection is notoriously difficult. Using Usutu virus (USUV) in the Netherlands as an example, we show how a computational framework can integrate diverse wildlife data sources to uncover hidden contributors to transmission. Our findings show that blackbirds, the most severely affected species, cannot sustain USUV transmission alone. Additional bird species, characterised by lower infection mortality and longer lifespans, are important for transmission and may protect more vulnerable species. This work emphasizes that studying transmission in a multi-host context is crucial for accurate outbreak predictions and effective interventions.

Introduction

Many emerging diseases arise from interactions between humans, animals, and ecosystems, where they are maintained in a complex ecological cycle [1]. These cycles often consist of different host species or host types, such as humans and animals or symptomatic and asymptomatic individuals. Distinguishing the contributions of each host type to observed outbreak dynamics is crucial to inform predictions, early detection, preparedness, and response to outbreaks. Contributions of different host species to transmission has been studied for several diseases and settings, such as minks and humans for SARS-CoV-2 [2], different bird species for avian influenza [3], cattle and wildlife for bovine tuberculosis [4] and wildlife reservoir hosts for plague [5]. Such analyses improve our understanding of the disease system and could also help inform and target surveillance strategies [6, 7] and (non-pharmaceutical) interventions, including vaccines where available [8–10]. Depending on each species' contribution to transmission, interventions may need to target multiple host species as e.g., for brucellosis [11] and rabies [12]. A better understanding of host contributions can also inform risk of geographical expansion of emerging pathogens and future changes in disease burden of established pathogens.

Disentangling contributions to disease transmission is notoriously complex. This is especially the case for wildlife diseases where often pathogens are capable of infecting multiple species, and pathogenicity and transmission potential can vary substantially between species [13]. In wildlife diseases, our ability to unravel these contributions is often hampered by the lack of high-quality information on population trends and distributions, patterns of infection and disease occurrence, and the lack of computational tools to integrate a wide range of data sources. Particularly during the emergence phase of a novel pathogen, detailed outbreak data may be scarce and biased towards humans. Several contributing species may therefore remain unidentified, even though they are affecting disease dynamics, constituting the so-called 'epidemiological dark matter' [14, 15]. Developing approaches capable of assessing the role of this dark matter in shaping transmission has been described as one of the main challenges for understanding multi-host disease dynamics [14].

A prime example of a virus where multiple, unidentified, host species may contribute to transmission is Usutu virus (USUV). USUV is a mosquito-borne virus, closely related to West Nile virus, that emerged in the Netherlands in the past decade [16]. The first bird infected with USUV virus in the Netherlands was detected in April 2016, with a substantial increase of reported dead Eurasian blackbirds (*Turdus merula*, hereafter: blackbird) observed later that year and in subsequent years [16, 17]. Multi-year surveillance conducted in the Netherlands by an extensive research network investigating arboviruses in wild birds revealed striking emergence patterns (Figure 1) [18]. Firstly, USUV appeared to have spread from South to North between 2016-2018. Secondly, this period was followed by several years with fewer detections, after which this increased again in 2022. USUV is transmitted in a cycle between mosquitoes and birds, with *Cx. pipiens* likely being the most important vector species in Europe [19]. Blackbirds have been particularly impacted by USUV, but the virus has been detected in many other bird species [18, 19] and serological evidence of infection has been found in a wide range of animals [18, 20]. While several animal species are susceptible to USUV infection, it is not clear whether, and to what extent, these hosts played a role in shaping USUV emergence and spread.

To characterize the role of host populations other than blackbirds in transmission dynamics, we developed a Bayesian inference framework in which mechanistic USUV transmission models were fitted to several sources of blackbird surveillance data. Through comparing these models, we disentangled the characteristics of a potential unobserved reservoir population. Using the best-fitting model we reconstructed the emergence over time and space and quantified each population's contribution to transmission over time.

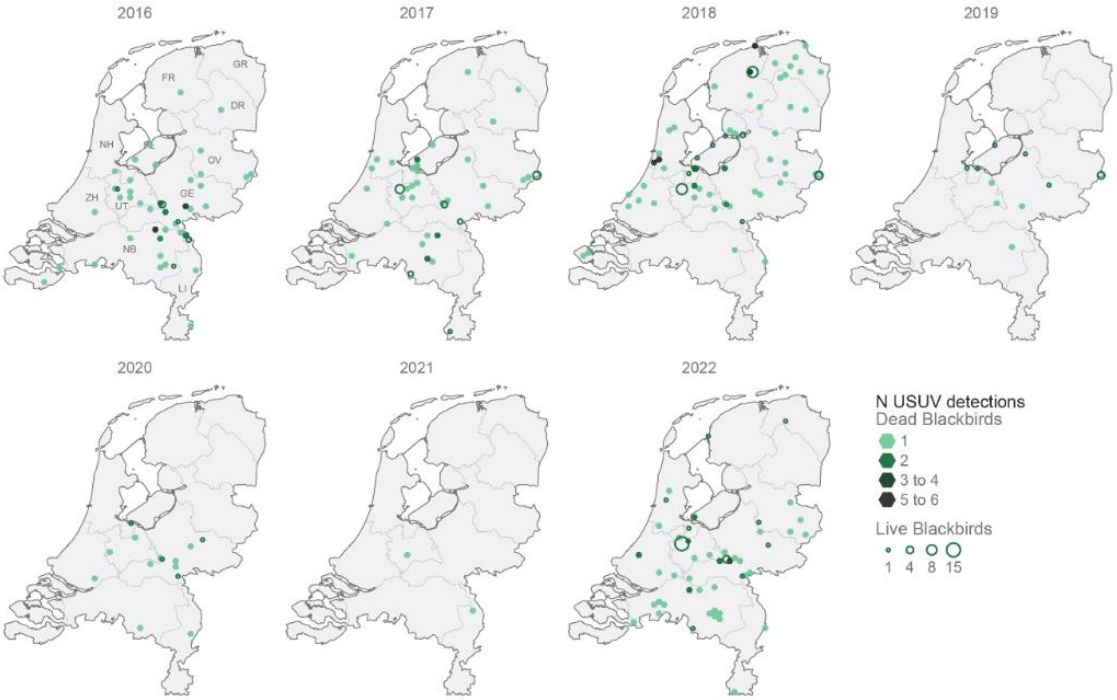

Figure 1: Spatio-temporal emergence pattern of USUV in the Netherlands, 2016-2022. Circular symbols indicate detections in live birds, with sizes proportional to the number of detections. Shading intensity in hexagonal grid cells (size: 30 km²) reflect the number of detections in dead free-ranging birds in that cell. Provincial borders are shown and are labelled with two-letter abbreviation in the first map. Adapted from Munger et al. 2024 [18].

Results

Trends in epidemiological surveillance data

Five sources of blackbird surveillance data were used to study USUV emergence between 2016-2022 [18]. Observations were filtered to align with the modelled transmission season (April to October). Surveillance data included infection prevalence (based on RT-PCR; n=2499) and seroprevalence in live blackbirds (n=1091), infection prevalence in dead blackbirds (n=284), blackbird population size, and reported dead blackbirds (n=3505). Infection prevalence in live blackbirds varied between years with the lowest observed prevalence in 2021 (0 positive cases) and highest in 2018 (0.09 95%CI 0.05-0.12). Prevalence in dead blackbirds was much higher and ranged from 0.10 (95%CI 0-0.22) in 2021 to 0.87 (95%CI 0.79-0.95) in 2018. Seroprevalence peaked in 2018 (0.22, 95%CI 0.16-0.27), which coincided with the lowest blackbird population size being observed in the following spring. Most dead birds were reported in 2016 (29% of the total across 2016-2022) (Supplementary figure 13).

Validation of inference approach

Before fitting our model to the surveillance data, we validated the inference framework against five simulated datasets using the blackbird-only model (Supplementary Material E). We found high agreement between true values and posterior medians (concordance coefficients 0.81-0.94) for the re-emergence rate, abundance scaling parameter, transmission probability bird-to-mosquito, and disease-induced mortality rate. Identifiability of regional-level historical force of infection (FOI) was poor (concordance coefficients <0.5). All parameters were therefore estimated at the national level going forward.

Characterising hidden host populations

To explore the potential role of host populations other than blackbirds in the emergence of USUV we developed four transmission models with different host population characteristics (Table 1) based on empirical data of mosquito- and bird abundance [21, 22], bird movement, and local temperature [23].

These models were fitted to the five surveillance datasets using Approximate Bayesian Computation. Models were compared based on the (normalised) distances between model predictions and observed data across the five datasets. Models that included an additional reservoir population (mean normalised distances 0.51-0.92) consistently outperformed the blackbird-only model (model A, mean normalised distances 0.96) (Figure 2E). Comparison of different reservoir population characteristics revealed that the observed patterns in blackbirds were best described by the presence of a reservoir population that does not die from infection and disperses further than blackbirds (model D). This model was able to capture both the South-to-North patterns and the reduced transmission in later years (Figure 2A-D) and showed the best fit to the data across four out of five datasets (Figure 2E, mean normalised distances = 0.51, compared to 0.67 for B, and 0.92 for C).

Sensitivity analyses showed that results of the best-fitting model (model D) were robust to assumptions regarding the location of virus introductions (mean normalised distance 0.53) and the spatial distribution of the reservoir population (mean normalised distance 0.53, Supplementary figure 19). Sensitivity analyses exploring the impact of uncertainty in blackbird movement distances (i.e., equal movement in breeding and post-breeding seasons) suggested that the increased dispersal required to explain the data falls within the uncertainty range of our blackbird movement estimates (mean normalised distance 0.52). All further analyses are based on the best fitting main model: model D. Inspection of model fits showed that this model was able to capture the trends in population size and immunity levels in blackbirds, but underestimated prevalence in 2017 and 2022 and did not capture trends in reported dead blackbirds (Supplementary Supplementary figure 16). Model fits to within-year trends are shown in Supplementary figure 18, model fits of all other models are shown in Supplementary Figure 20-23, and further inference diagnostics can be found in Supplementary Material G.

Posterior estimates showed that the average adult lifespan of the modelled additional reservoir population was 6.8 years (95% CI 1.8 – 12.2). This population received 34 times (95%CI 26 – 48) more bites than the blackbird population per day, due to differences in population size and/or mosquito biting preference. Posterior distributions were largely robust across model versions showing high degree of overlap in 95% highest density intervals, especially across models D and S1-3 (Supplementary Table 7).

Table 1: Specification of model versions

	Virus introduction	Host species	Characteristics other host species			
			Infection mortality ratio	Lifespan	Dispersal distance	Population distribution
Model A: Blackbird only						
A	South	Blackbird	NA	NA	NA	NA
Model B: Reservoir host: increased dispersal						
B	South	Blackbird & other	Blackbird-like	Blackbird-like	Increased	Blackbird-like
Model C: Reservoir host: no infection mortality & estimated lifespan						
C	South	Blackbird & other	Zero	Estimated	Blackbird-like	Blackbird-like
Model D: Reservoir host: increased dispersal & no infection mortality & estimated lifespan						

D	South	Blackbird & other	Zero	Estimated	Increased	Blackbird-like
Sensitivity analyses*						
Model S1: Introductions country-wide						
S1	Everywhere**	Blackbird & other	Zero	Estimated	Increased	Blackbird-like
Model S2: Uniform spatial distribution reservoir host						
S2	South	Blackbird & other	Zero	Estimated	Increased	Uniform
Model S3: Alternative movement distances						
S3	South	Blackbird with alternative dispersal*** & other	Zero	Estimated	Blackbird-like with alternative dispersal**	Blackbird-like

* Sensitivity analyses were based on model D, because this was the best-fitting model from options A-D.
** In model S1, the virus was successfully introduced (i.e. leading to an infected mosquito) each day between April and mid-October in 2016 in randomly chosen locations throughout the country. In all other models, introductions happened at one-third this rate to keep the number of introductions in the South equal between all models.
** In the 'blackbird-like with alternative dispersal' scenario, post-breeding season movement was increased to equal breeding season movement.

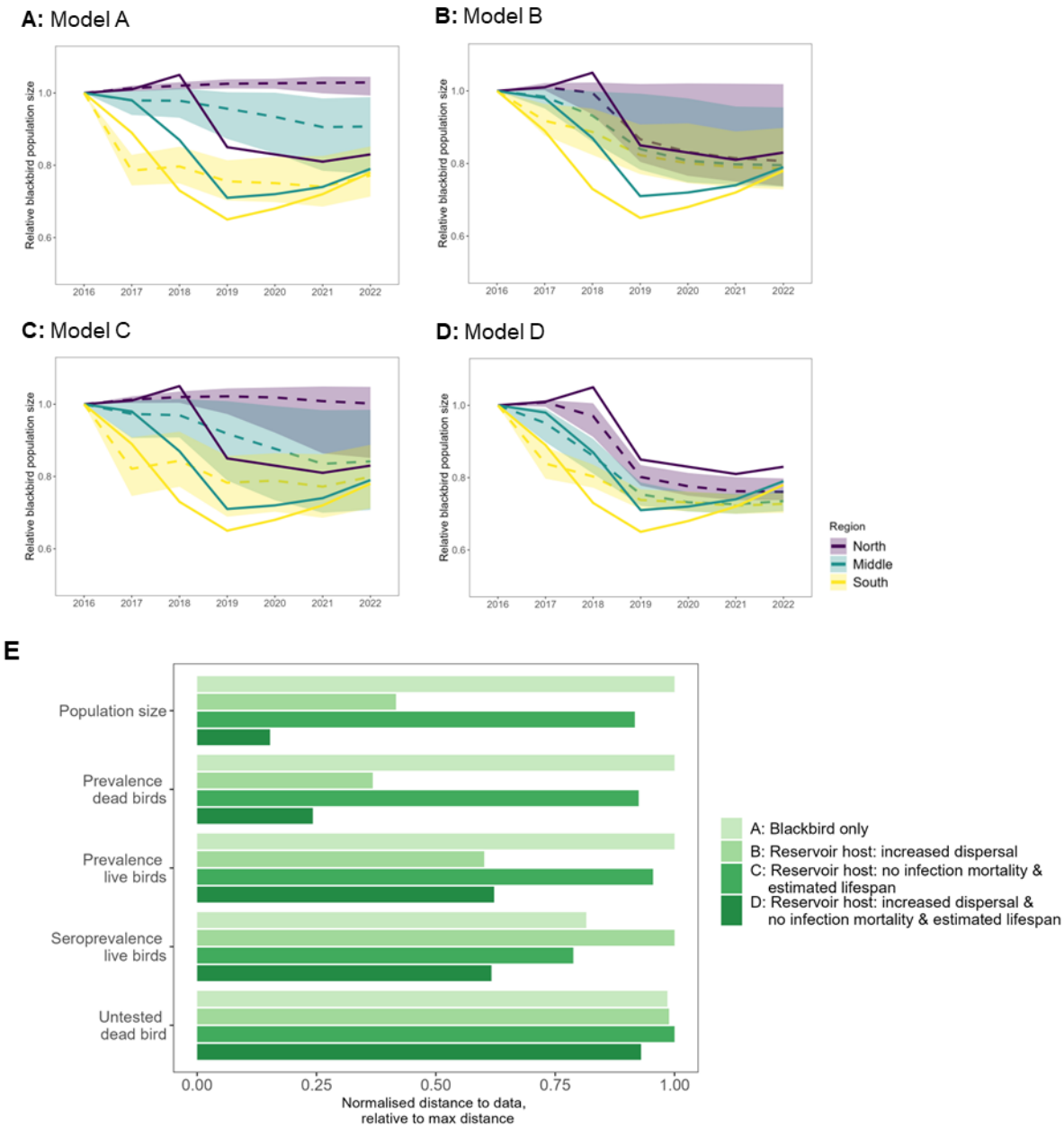

Figure 2: Comparison of model versions. A-D) Visual fit of simulated data (dashed lines with 95% prediction interval) to observed data (solid lines) for the blackbird population size. Results are shown for the four main models A to D. E) Comparison of model fits between main model versions. Comparisons were based on distances between observed and simulated data for each data set. For each data set, distances were normalised by dividing each model's distance by the maximum across all model versions. A normalised distance of 1 thus indicates that this model showed the largest distance between observed and simulated data (i.e. worst fit). Lower normalised distances indicate a better fit to the data.

Reconstruction of USUV emergence

In addition to the role of reservoir host populations, we also examined other determinants of the USUV outbreak. The best-fitting model showed an estimated infection mortality ratio for blackbirds of 76% (95%CI 71-80). While the first RT-PCR-positive bird was found in 2016, undetected transmission prior to 2016 cannot be ruled out. We therefore aimed to estimate the level of immunity in 2016, but found that evidence of transmission prior to 2016 using our model was inconclusive (historical FOI 0.10, 95%CI $1.8*10^{-4}$ – 0.25). Additionally, we quantified the annual USUV re-emergence rate, representing the possibility of local overwintering and/or re-introductions from migratory birds. This rate was estimated at 20.3% (95%CI 7.9-29.6), indicating that USUV prevalence in mosquitoes at the start of the new season

(April) is around 80% lower than at the end of the previous season (mid-September). Posterior distributions for all parameters and model versions are available in Supplementary Table 7.

We used our best-fitting model to reconstruct the emergence of USUV into the Netherlands. Prevalence in live and dead blackbirds generally peaked in August and September, matching the trends in observed data (Figure 3A & B). In our model, highest monthly average prevalence was estimated in August 2018 at 3.4% (95%CI 2.8-4.0) in live birds and 70.8% (95%CI 64.6-75.9) in dead blackbirds. While the mean prevalence in live blackbirds tended to be highest in juveniles (0.7%, 95%CI 0.6-0.9, adults: 0.5%, 95%CI 0.4-0.7), prevalence in dead blackbirds was highest in adults (31.9%, 95%CI 25.0-39.3, juveniles: 18.7%, 95%CI 14.9-22.6). Seroprevalence generally peaked in October and was on average 4.8 times higher in the modelled alternative reservoir population (68.3%, 95%CI 58.3-74.4) compared to seroprevalence in blackbirds (14.4%, 95%CI 11.3-18.0) (Supplementary figure 17).

We calculated basic reproduction numbers (R_0), indicating the number of secondary infections resulting from one infectious individual in a fully susceptible population, and effective reproduction numbers (R_e), indicating the number of secondary infections when accounting for immunity in the population. The annual mean R_e was highest in 2016, when immunity was still limited, and lowest in 2019 (Figure 3C). The R_e tended to get above 1 at the end of May, peaked in July and dropped below 1 in early September, when mosquitoes started entering diapause. Differences in R_e between regions were small (R_e: North 3.4 (95%CI 2.7-4.9), Middle 3.0 (95%CI 2.5-5.0), South 2.9 (95%CI 2.3-4.7)) (Supplementary figure 31-32).

Contributions of different host populations to transmission

To disentangle contributions to transmission from the different host populations, we calculated reproduction numbers for each transmission cycle, so-called partial reproduction numbers (Supplementary figure 30). We found that the reservoir-mosquito cycle contributed more to overall transmission than the blackbird-mosquito cycle. The R_e of the blackbird-mosquito cycle during the transmission season was 0.08 (95%CI 0.06-0.12), meaning that USUV could not persist in blackbirds alone. With an R_e of 3.0 (95%CI 2.3-4.1), USUV could persist in the reservoir-mosquito cycle (Figure 3D). Juvenile blackbirds contributed about two times more to transmission than adult blackbirds (juvenile R_e 0.07 (95%CI 0.05-0.10), adult R_e 0.04 (95%CI 0.03-0.05) (Figure 3D).

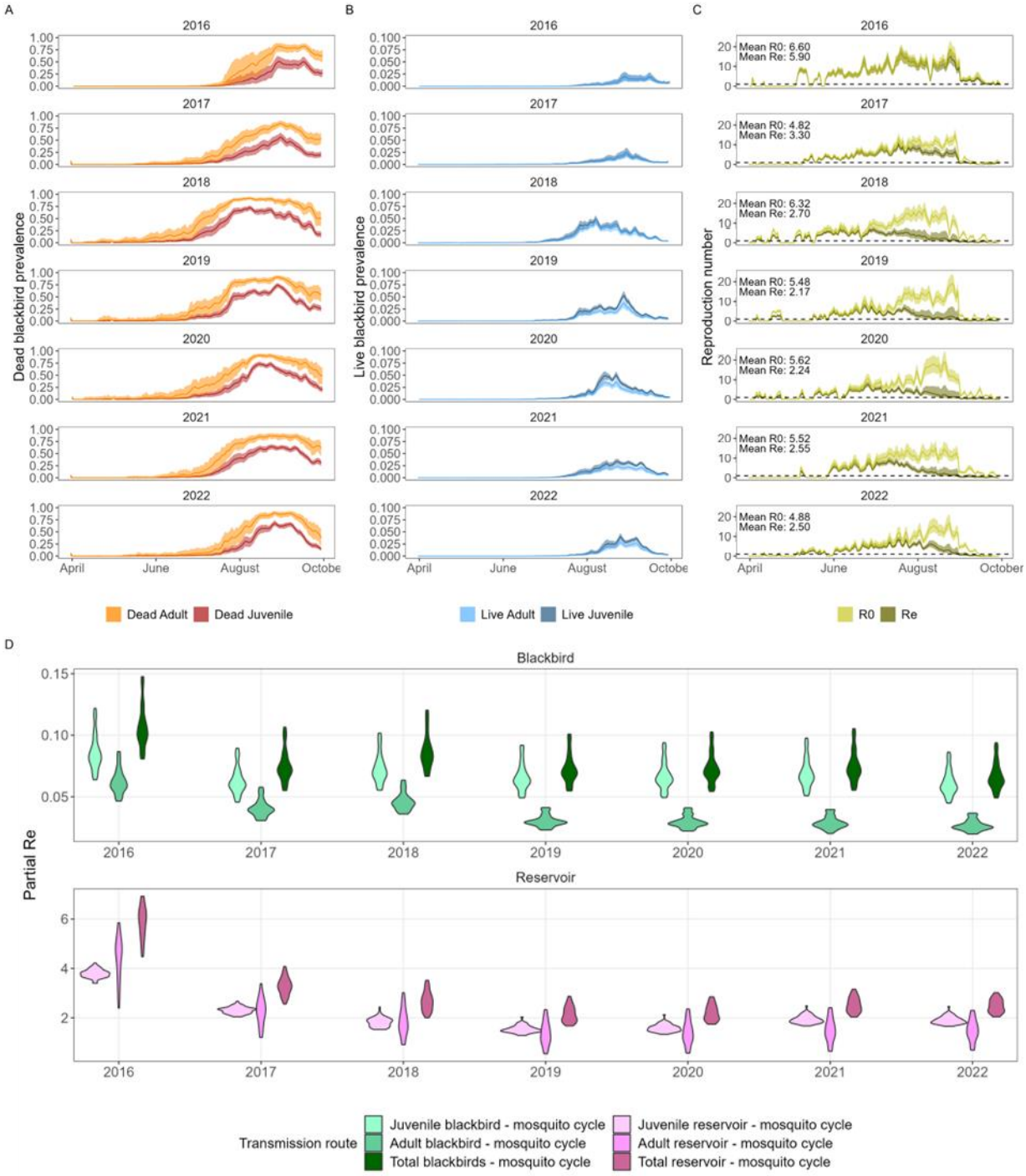

Figure 3: Model outputs generated from 100 simulations using random draws from parameter sets from posterior distributions. A) Prevalence during the transmission season in dead blackbirds split by age group. B) Prevalence during the transmission season in live blackbirds split by age group. C) R_0 and R_e during the transmission season. D) Partial effective reproduction numbers per transmission route averaged over the transmission season. Results are shown per transmission season from April to October while averaging across all locations. In plots A-C, solid lines indicate mean values and shaded areas show 95% prediction intervals.

Discussion

Understanding contributions to transmission of different host types is an important step towards developing effective surveillance and control strategies. Our ability to disentangle host contributions in wildlife is generally limited by the availability of data on host populations as well as difficulties in collecting surveillance data across multiple species. These barriers are even more prominent for emerging wildlife diseases where epidemiological information and outbreak data are scarce. Here, we integrated five sources of surveillance data with data on vector and host abundance, movement, and local temperature in a Bayesian modelling framework. Using USUV as a case study, we showed that ignoring the multi-host context of transmission strongly impacts estimated outbreak dynamics. Specifically, failing to account for the build-up of immunity in alternative host populations hampers the model's ability to accurately capture multi-annual trends. We found that while blackbirds were strongly impacted by the virus, they could not by themselves contribute sufficiently to the population-level build-up of immunity, nor to the spread needed to explain the spatial and multi-annual patterns of emergence. We used the inference framework to characterise the unobserved reservoir population as having a longer lifespan, little disease-induced mortality, and likely a larger home range than blackbirds.

Contributions from different host populations

We found that, during the first recorded outbreak of USUV in the Netherlands, one or more host species in addition to blackbirds played a role in transmission. Previous studies highlighted evidence of infection in a wide range of animal hosts [18–20]. Several papers have explored contributions of and interactions between host stages and/or species for the closely related West Nile virus from a theoretical perspective, highlighting the large impact that such interactions can have on outbreak dynamics [24–29]. However, this impact has not been demonstrated before from real-life outbreak data. We found that the reproduction number for the blackbird-mosquito cycle was below 1 (maximum value 0.32 (95%CI 0.23-0.45)) during the whole transmission season, suggesting that USUV persisted due to the competence and abundance of other populations. An important driver of the difference in contribution between the two host groups was the estimated distribution of mosquito bites. The proportion of bites on each host is a consequence of both host preference and relative abundance, which we could not disentangle in our analysis. Our estimated distribution of bites (1-2% on blackbirds) is consistent with observations in the field (0-9% of bites on blackbirds) [30]. However, this model-based estimate is sensitive to assumptions around transmission probabilities, which we assumed to be the same for the reservoir population as for blackbirds. It is important to note that these findings do not imply that USUV transmission can only be sustained in the presence of other competent bird species, but that this depends on how many mosquito bites blackbirds receive, which is a function of the composition of the total population mosquitoes feed on [30, 31].

Immunity in the reservoir population

High level of immunity in the reservoir population was found to be an important explanation of observed transmission dynamics. While the basic reproduction number remained high each year, the effective reproduction number reduced as the outbreak spread across the country. The strong decline in the effective reproduction number in the (adult) reservoir population in the first three years indicates that immunity in this population reduced USUV transmission in later years and thereby protected the blackbird population from further decline. An Austrian study reported an USUV seroprevalence of 8.5% across several wild bird species in 2003-2004, but seroprevalence had increased to 54% even before the transmission seasons of 2005-2006 [32]. Also here, the authors hypothesised that herd immunity has led to a reduction in USUV-related mortality. In Spain, mean annual WNV seropositivity levels ranged from 5 to 69% [33]. These studies show that heterogeneity in reported seroprevalence levels is large, with estimates varying both between and within years. Lifespan of the reservoir population also affects immune dynamics. Seroprevalence and reservoir lifespan estimates (which showed large uncertainty in this study) could be improved as longer time series of surveillance data become available.

Identifying the reservoir population

Existing literature can be combined with surveillance data available on other bird species to start identifying which species are represented in the reservoir population. Of the four species with more than ten samples in 2005 in an Austrian study [32], all showed USUV seroprevalence estimates of around 50% or higher (blackbirds, Eurasian blackcaps (*Sylvia atricapilla),* Ural owls *(Strix uralensis),* and European robins *(Erithacus rubecula)*). However, only a subset of these birds were live captured wild birds and a significant proportion were captive birds and/or sick, injured, or dead. In the Netherlands, annual seroprevalence levels of that order of magnitude were not observed in any species, but species-specific sample sizes were often limited and estimates are sensitive to the timing of sampling. Highest seroprevalence levels among commonly sampled species in 2016-2022 were found in Carrion crows *(Corvus corone)* (13.7%, n=51, some of which were sick), Eurasian magpies *(Pica pica)* (14.1%, n=64), and Eurasian collared doves *(Streptopelia decaoto)* (11.1%, n=36) [18]. While the impact of USUV infection is unknown for most of these species, studies indicated that magpies do not show clinical symptoms after USUV infection [34]. Magpies also live somewhat longer than blackbirds, typically five years after reaching breeding age [35]. Other species found positive for USUV in the Netherlands disperse further, such as crows and doves [36, 37]. Enhancing sampling in species with high seropositivity levels, experimental infections to assess competence and infection response, supplemented by demographic characteristics, could shed more light on the identity of species constituting the reservoir population.

Temporal trends in transmission

We were able to reproduce the large outbreaks observed during the first three years of emergence, after which transmission was sustained at a lower intensity. We estimated that the effective reproduction number generally dropped below one after early September. Variation in basic reproduction numbers within and between years were mainly driven by mosquito population size and mean daily temperature, and to a smaller extent by bird population size. Reproduction numbers were estimated to be highest in 2016 and 2018, coinciding with the highest estimated mosquito abundance in 2016 and highest spring and summer temperatures in 2018. In 2016, a large USUV outbreak was observed in Germany during which the virus spread towards North Rhine-Westphalia [38, 39], a region to the southeast of the Netherlands. The high reproduction numbers in 2018 coincided with the largest observed WNV outbreak to that date in Europe [40]. These findings highlight a possible correlation in arbovirus transmission across regions in Europe. Transmission season was shortest in 2021, where the reproduction number was not consistently above one until June, coinciding with the coldest spring of the study period. While some of the surveillance data sources showed increased transmission in 2022 compared to the previous years, this was not captured by the model, mostly because predicted mosquito abundance was lowest during this year. Limitations that may have impacted the predicted annual variation in transmission include the simplifying assumption of a constant number of newborn birds each year, while variation might occur due to environmental conditions [41], the assumption of a constant virus re-emergence rate each year, and remaining biases in surveillance data. We estimated the re-emergence rate (around 20%) as the proportion of the USUV prevalence in mosquitoes that persists to the next spring, representing the possibility of local overwintering and/or re-introductions from migratory birds. While we estimated a constant rate, this may be affected by winter temperatures [42] and variation in bird migration patterns, among others.

Implications for surveillance and predictions

Our findings indicate that blackbirds are useful as a sentinel species for USUV circulation due to their high infection mortality rate. The high prevalence in dead blackbirds makes sampling of dead blackbirds an efficient surveillance strategy to detect circulation. However, to better identify which other species can contribute to transmission, frequent sampling of a wider range of species is necessary. Longitudinal serological surveillance would be most appropriate to identify reservoir species, as they might not display increased mortality. Such information could be useful when making projections about future transmission risks and when predicting the suitability for USUV circulation. The large contribution of alternative host species implies that also regions with low blackbird density may well be suitable for

USUV transmission, but this might remain undetected if surveillance is focused on dead bird reporting, as is the case in many other European countries. Additionally, the model could be employed to evaluate current surveillance strategies by adding these into the model and provide recommendations regarding sampling intensity, timing, and location for different surveillance systems.

Importance of multiple data sources

Using multiple sources of data for inference is one of the key challenges in epidemiological modelling [43]. We addressed several obstacles related to synthesising diverse datasets. A common challenge in the use of multiple datasets for inference is weighing observations that are not on the same scale. We addressed this by defining acceptance thresholds for each dataset individually thereby placing equal weight on each dataset and only accepting parameters that simultaneously met the threshold for all datasets. This allowed for the model to be fitted to multiple aspects of an outbreak, representing different characteristics of the disease system, including population impact, infection levels in both live and dead hosts, and immunity build-up. Additionally, these data sources represented varying levels of temporal aggregation of the system. By simultaneously calibrating to multiple datasets, the impact of bias in one of the datasets and the risk of overfitting is reduced. Moreover, when known, we were able to account for the observation process by explicitly reproducing this such as for the seroprevalence and live blackbird prevalence datasets. The use of summary statistics, in contrast to likelihood functions, increased flexibility in the definition of optimisation function and these could therefore be designed such that they are more robust to imperfect sampling compared to the full dataset. The inference validation analysis showed that our framework was able to correctly estimate unknown parameters from simulated data. These approaches enhance the usability of datasets, that would be insufficient on their own to address specific epidemiological questions. While more complete and larger datasets would be recommended for such analyses, this is unrealistic in the context of wildlife surveillance. With the increasing availability of novel surveillance data streams, possibilities to collect multiple types of data on the same outbreak are expanding. This highlights the importance of developing and evaluating computational approaches capable of integrating different data types.

Conclusions

This study showed how modern modelling approaches can integrate diverse data sources to uncover drivers of transmission that could not be identified in a traditional outbreak investigation. Here, this approach was applied to USUV, a newly emerging multi-host virus in the Netherlands, where the unique availability of multiple streams of surveillance data during the emergence period made such analyses possible. Our results highlight the importance of considering multiple host populations to understand outbreak dynamics. Ignoring the multi-host context of disease transmission can have implications for the projected effectiveness of intervention strategies or accuracy of future predictions. Advances in novel data streams and modelling techniques present highly promising developments in our ability to unravel transmission processes and characterise ‘epidemiological dark matter’.

Methods

Model overview

We created a stochastic compartmental metapopulation model to simulate transmission of USUV between *Culex pipiens* mosquitoes and blackbirds in the Netherlands from 2016 to 2022 (Figure 4). Blackbirds were chosen as the main host species for this study, because they showed highest USUV prevalence among live birds [18] and showed high mortality following USUV transmission [16, 17]. To explore the potential role of other hosts, we also created model variants that included an additional host population, representing unidentified USUV-competent species. Both the host and vector populations were divided into compartments based on their infection status: susceptible, exposed, infected, recovered, and dead compartments for birds, and susceptible, exposed, and infected compartments for mosquitoes. The model's starting conditions were determined by the historical FOI (see 'Estimated parameters'). Birds can get infected when they get bitten by an infectious mosquito. Mosquitoes can get infected when they bite an infectious bird. We assumed host frequency-dependent transmission. This follows from the assumption that the vector biting rate is independent of host density, and the biting rate experienced by hosts increases with vector density [44, 45]. The mosquito population dynamics, extrinsic incubation period, and biting rate were temperature-dependent. The full set of equations and parameter values are described in Supplemental Material A.

The temporal resolution of the model was one day. We used a 5 by 5 km grid structure and assumed that birds and mosquitoes were homogeneously distributed within a grid cell. Bird and mosquito abundance differed between grid cells. Virus transmission occurred within a grid cell and cells were connected through bird movements. We distinguished daily foraging movement patterns from seasonal natal and breeding dispersal [46, 47]. To allow for different movement patterns across life stages and seasons, we divided the year into breeding season (April-July) and post-breeding (July-October) and the bird populations into juveniles (from fledging until the next breeding season) and adults (birds older than one year). Only bird movement during the virus transmission season was included (April to October), as movement outside this season was assumed not to affect transmission. Similarly, blackbird spring and autumn migration was not included explicitly because this largely occurs outside the transmission season and Dutch blackbirds have almost completely stopped migrating over the past decades [48]. Movement of mosquitoes between cells was ignored due to a lack of high-quality evidence available for parameterisation [49]. The model was run continuously from April 2016 to the end of 2022, with the virus re-emerging in the mosquito population each year, representing the possibility of local overwintering and/or re-introductions from migratory birds.

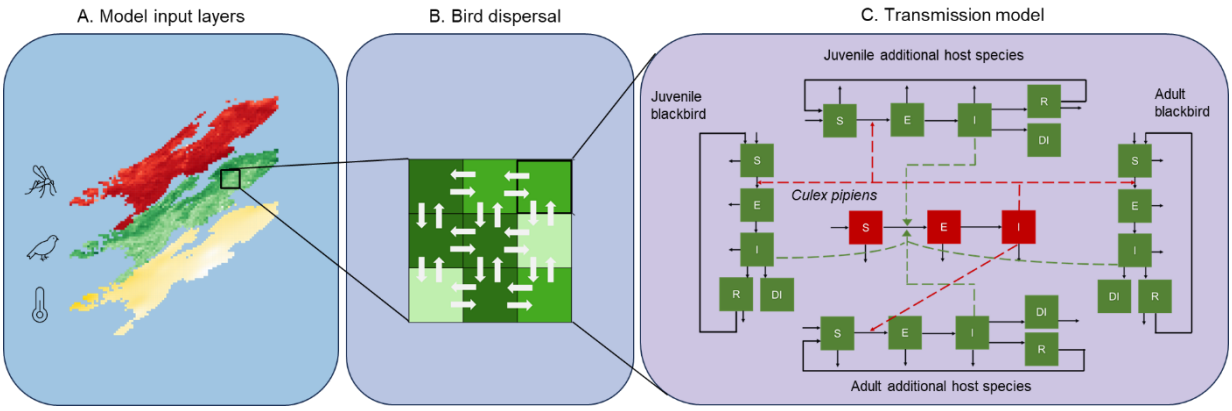

Figure 4: ***Model overview.***
The country is divided into equally sized 5x5km grid cells, which vary with respect to bird and mosquito abundance as well as temperature. Birds disperse between cells. Transmission occurs within a grid cell. In the SEIR-model, dark arrows represent transitions between infection states, while dashed arrows represent the link to the source of transmission. S = susceptible, E = exposed, I = infectious, R = recovered, DI = dead from infection.

Non-connected outward pointing arrows represent natural death of the animal. Non-connected inward pointing arrows represent births.

Input layers

Bird and mosquito abundance

Relative blackbird abundance was obtained for each grid cell from Dellar et al. [21]. In this paper, Random Forest models were fitted to blackbird point count data (n=183,123 observations) from the Netherlands (Meetnet Urbane Soorten [46], Meetnet Agrarische Soorten [47] and Common Bird Census [48] from Sovon Vogelonderzoek Nederland (Dutch Centre for Field Ornithology)) and France (Common Bird Monitoring Scheme [49]) in the period 2001-2016, using a set of environmental and climatic predictors. Relative *Culex pipiens* abundance was obtained for each day and each grid cell from Krol et al. [22]. Here, data on female mosquito trap counts was obtained from the National Mosquito Survey 2010-2013 [54] and the MODIRISK project [55]. Random Forest models were fitted to female mosquito count data including a set of land cover, environmental, and climatic predictors. Estimates for both blackbird and mosquitoes reflect relative abundance and were scaled proportional to each other using a scaling parameter (see 'Estimation parameters').

Bird movements

Two movement patterns were distinguished in the model, representing daily movements and seasonal dispersal. Daily movements include foraging-type movements often within the bird's home range, i.e. the area the bird regularly traverses around in its territory. In the model, this is reflected as a contribution to the FOI experienced in other grid cells. In addition to daily movements, we included seasonal dispersal that represents the search for a new nest location. Seasonal dispersal takes place during the change from breeding to post-breeding season in early July, whereby birds can move to a different grid cell. We quantified both the daily and seasonal blackbird movement patterns by fitting dispersal kernels to ringing and recovery data of blackbirds ringed and recovered in the Netherlands collected by Vogeltrekstation NIOO-KNAW. This resulted in a median daily movement distance of 143 m (inter-quartile range 19 - 692) during the breeding season and 29 m (inter-quartile range 4 – 129) during the post-breeding season. Seasonal dispersal distances were larger and estimated at a median distance of 377 m (inter-quartile range 95 - 1114) for juveniles and 180 m (inter-quartile range 19 – 1062) for adults. We constructed movement matrices by sampling from these dispersal kernels assuming rotational symmetry (Supplementary Material B). For the additional reservoir population we explored an additional movement scenario with a median distance of 1,016 m for breeding season and 323 m for post-breeding season (Supplementary Material B), seasonal movement was not included.

Temperature data

Average daily temperature data in the period 2016-2022 were obtained from the Royal Meteorological Institute (KNMI), with a 1x1 km spatial resolution [23].

Abundance and temperature data were resampled into the model grid using bilinear interpolation. A visual overview of bird and mosquito abundance as well as monthly temperature values can be found in Supplementary Figure 5.

Inference

Data sources

The model was calibrated to five sources of surveillance data collected on blackbirds: 1,2) PCR and seroprevalence in live blackbirds, 3) reported dead blackbirds, 4) PCR prevalence in a subset of these dead blackbirds, 5) annual blackbird population size. Further details of these data sources can be found in supplementary material C and in [18].

Approach

We used an Approximate Bayesian Computation approach using a Sequential Monte Carlo sampler (ABC-SMC) to calibrate our model to surveillance data [56]. This approach allows for complex transmission models to be fitted to data by using summary statistics, thereby avoiding having to explicitly define likelihood functions [57, 58]. In ABC-SMC, estimation of the posterior distribution is achieved sequentially by constructing intermediate distributions in each generation, converging towards the final posterior distribution. After each model iteration using proposed parameters, model output is compared to the data using summary statistics. Summary statistics each represent different epidemiological aspects of the outbreak. The parameter set is accepted if the distances between the model and data summary statistics are below their respective thresholds, where the thresholds become progressively stricter each generation based on results from the previous generation. For each model, we ran three chains of 200 particles and stopped when the acceptance rate reached 5% or less.

We used five summary statistics, one for each type of surveillance data: seroprevalence in live blackbirds, PCR prevalence in live blackbirds, and PCR prevalence in dead blackbirds for each month and region (North, Middle, South (Supplementary figure 12) as well as the annual blackbird population size relative to 2016 and the relative number of reported dead blackbirds per year within each region (Supplementary figure 13). More details on the inference approach can be found in Supplementary Material D.

Estimated parameters

The following parameters were estimated: 1) abundance scaling parameter, this converts the host and vector abundance to be on the same scale, meaning that their ratio reflects the vector-to-host ratio, 2) re-emergence rate, the fraction of the USUV prevalence in mosquitoes in September that persists to the subsequent spring, 3) disease-induced mortality rate in blackbirds, 4) transmission probability bird-to-mosquito, 5) historical FOI by region (North, Middle, South), to quantify transmission prior to first detection leading to non-zero immunity levels in 2016. For the model versions including an additional reservoir population, also this population's natural mortality rate and the distribution of mosquito bites between blackbirds and the reservoir population were estimated. For a more detailed description of the parameters, including the priors, see Supplementary Material D. To validate the ability and accuracy of our inference algorithm, we simulated data mimicking the surveillance data available with known parameter values using the blackbird-only model. We evaluated the ability of our model framework to estimate these parameter values using five simulated datasets.

Model comparisons and analyses

Four models (A-D) were created, which differed with respect to the presence and characteristics of an alternative reservoir population (Table 1). For all models, the historical FOI was set to be the same across the country. We assumed the virus was introduced in the South as that appeared to be the first region where transmission occurred. Additionally, we developed three sensitivity analyses (models S1-S3) based on the best-fitting model to explore sensitivity to the location of initial virus introductions (S1), to the spatial distribution of the reservoir populations (S2) and to uncertainty in our blackbird dispersal estimates (S3). In model S1, the virus was successfully introduced (i.e. leading to an infected mosquito) each day between April and mid-October in 2016 in randomly chosen locations throughout the country. In all other models, introductions happened at one-third this rate to keep the number of introductions in the South equal between all models. Models were compared based on their distances between observed and simulated summary statistics calculated in the last generation of the ABC algorithm, where accepted particles represent the best approximation of the posterior distribution. To ensure all summary statistics' distances were on the same scale, for each summary statistic separately we normalised the summed distances by dividing these by the maximum summed distances across all model versions.

Using the best fitting model, we ran 100 simulations using sampled parameter sets from the posterior distributions and calculated prevalence, seroprevalence, and (partial) basic (R_0) and effective (R_e)

reproduction numbers for each day and grid cell. Reproduction numbers were calculated using the Next Generation Matrix approach [59] (Supplementary Material H).

Funding statement

This publication is part of the project 'Preparing for Vector-Borne Virus Outbreaks in a Changing World: a One Health Approach' (NWA.1160.18.210), which is (partly) financed by the Dutch Research Council (NWO)). This work used the Dutch national e-infrastructure with the support of the SURF Cooperative using grant no. EINF-9367.

Acknowledgements

We would like to thank all volunteers at the bird ringing stations across the Netherlands for their efforts in catching and sampling birds. We would also like to thank all people involved in the coordination of these surveillance schemes, specifically Judith van den Brand, as well as those involved in the laboratory analyses. We are grateful to the members of the One Health PACT work package 3 and 4 for their helpful discussions and ideas.

Author contributions: MdW: conceptualisation, methodology, software, formal analysis, visualisation, data curation, writing – original draft, writing – reviewing and editing. **GB**: methodology, software, writing – reviewing and editing. **MD**: formal analysis, writing – reviewing and editing. **EM**: data curation, writing – reviewing and editing. **LK**: formal analysis, writing – reviewing and editing. **NA**: data curation. **JvI**: formal analysis, data curation, writing – reviewing and editing. **HvdJ**: conceptualisation, data curation, writing – reviewing and editing. **MK**: funding acquisition, conceptualisation, writing – reviewing and editing. **MdJ**: conceptualisation, methodology, supervision, writing – reviewing and editing. **RS**: data curation, writing – reviewing and editing. **QtB**: conceptualisation, methodology, supervision, writing – original draft, writing – reviewing and editing.

Competing interest statement: The authors declare that they have no competing interests.

Data availability statement: Data on dead reported birds is available upon request at https://www.sovon.nl/tellen/telprojecten/dode-vogel-melden. Population trends for the Dutch blackbird population were derived from a national breeding bird monitoring scheme [60]. The datasets on live and dead free-ranging birds analysed in this study will be made available in the BioStudies database (http://www.ebi.ac.uk/biostudies) under accession numbers [accession numbers] and can be accessed via [Pathogens Portal Netherlands, currently in advanced development].

References

1. Adisasmito WB, Almuhairi S, Behravesh CB, et al (2022) One Health: A new definition for a sustainable and healthy future. PLoS Pathog 18:e1010537

2. Munnink BBO, Sikkema RS, Nieuwenhuijse DF, et al (2021) Transmission of SARS-CoV-2 on mink farms between humans and mink and back to humans. Science (1979) 371:172–177

3. Brown VL, Drake JM, Stallknecht DE, Brown JD, Pedersen K, Rohani P (2013) Dissecting a wildlife disease hotspot: the impact of multiple host species, environmental transmission and seasonality in migration, breeding and mortality. J R Soc Interface. https://doi.org/10.1098/RSIF.2012.0804

4. Crispell J, Zadoks RN, Harris SR, et al (2017) Using whole genome sequencing to investigate transmission in a multi-host system: Bovine tuberculosis in New Zealand. BMC Genomics 18:1–12

5. Webb CT, Brooks CP, Gage KL, Antolin MF (2006) Classic flea-borne transmission does not drive plague epizootics in prairie dogs. Proc Natl Acad Sci U S A 103:6236–6241

579 6. ten Bosch QA, Clapham HE, Lambrechts L, et al (2018) Contributions from the silent
580 majority dominate dengue virus transmission. PLoS Pathog.
581 https://doi.org/10.1371/JOURNAL.PPAT.1006965

582 7. Colman E, Holme P, Sayama H, Gershenson C (2019) Efficient sentinel surveillance
583 strategies for preventing epidemics on networks. PLoS Comput Biol 15:e1007517

584 8. Powers KA, Ghani AC, Miller WC, Hoffman IF, Pettifor AE, Kamanga G, Martinson FE,
585 Cohen MS (2011) The role of acute and early HIV infection in the spread of HIV and
586 implications for transmission prevention strategies in Lilongwe, Malawi: a modelling
587 study. The Lancet 378:256–268

588 9. Streicker DG, Fenton A, Pedersen AB (2013) Differential sources of host species
589 heterogeneity influence the transmission and control of multihost parasites. Ecol Lett
590 16:975–984

591 10. Flasche S, Lipsitch M, Ojal J, Pinsent A (2020) Estimating the contribution of different
592 age strata to vaccine serotype pneumococcal transmission in the pre vaccine era: A
593 modelling study. BMC Med 18:1–12

594 11. Beauvais W, Musallam I, Guitian J (2016) Vaccination control programs for multiple
595 livestock host species: An age-stratified, seasonal transmission model for brucellosis
596 control in endemic settings the LCNTDR Collection: Advances in scientific research for
597 NTD control. Parasit Vectors 9:1–10

598 12. Fitzpatrick MC, Hampson K, Cleaveland S, Meyers LA, Townsend JP, Galvani AP (2012)
599 Potential for Rabies Control through Dog Vaccination in Wildlife-Abundant
600 Communities of Tanzania. PLoS Negl Trop Dis 6:e1796

601 13. Woolhouse MEJ, Taylor LH, Haydon DT (2001) Population biology of multihost
602 pathogens. Science (1979) 292:1109–1112

603 14. Buhnerkempe MG, Roberts MG, Dobson AP, Heesterbeek H, Hudson PJ, Lloyd-Smith JO
604 (2015) Eight challenges in modelling disease ecology in multi-host, multi-agent
605 systems. Epidemics 10:26–30

606 15. Orton RJ, Wright CF, Morelli MJ, Juleff N, Thébaud G, Knowles NJ, Valdazo-González B,
607 Paton DJ, King DP, Haydon DT (2013) Observing micro-evolutionary processes of viral
608 populations at multiple scales. Philosophical Transactions of the Royal Society B:
609 Biological Sciences. https://doi.org/10.1098/RSTB.2012.0203

610 16. Rijks JM, Kik M, Slaterus R, et al (2016) Widespread Usutu virus outbreak in birds in
611 The Netherlands, 2016. Eurosurveillance. https://doi.org/10.2807/1560-
612 7917.ES.2016.21.45.30391

613 17. Montizaan M, Kik M, Rijks J, et al (2019) Nature Today | Opnieuw dode vogels door
614 usutuvirus in Nederland; nog onverklaarde daling meldingen dode merels.
615 https://www.naturetoday.com/intl/nl/nature-reports/message/?msg=25571.
616 Accessed 24 Aug 2020

617 18. Munger E, Atama N, Irsel J van, et al (2024) Emergence and Dynamics of Usutu and
618 West Nile Viruses in the Netherlands, 2016-2022. bioRxiv 2024.12.16.628479

619 19. Nikolay B (2015) A review of West Nile and Usutu virus co-circulation in Europe: how
620 much do transmission cycles overlap? Trans R Soc Trop Med Hyg 109:609–618

621 20. Angeloni G, Bertola M, Lazzaro E, et al (2023) Epidemiology, surveillance and diagnosis
622 of Usutu virus infection in the EU/EEA, 2012 to 2021. Eurosurveillance 28:2200929

623 21. Dellar M, Sierdsema H, van Bodegom PM, Schrama MJJ, Geerling G (2024) The future
624 abundance of key bird species for pathogen transmission in the Netherlands. bioRxiv
625 2024.10.14.617534

626 22. Krol L, Dellar M, Ibáñez-Justicia A, Schrier G van der, Schrama M, Geerling GW,
627 Bodegom PM van (2024) Combined effects of future climate and land use change on
628 mosquitoes: The distribution of Culex pipiens under One Health scenarios in the
629 Netherlands. https://doi.org/10.21203/RS.3.RS-5298493/V1

630 23. (2015) Temperature - gridded daily mean temperature in the Netherlands. In: KNMI.
631 https://dataplatform.knmi.nl/dataset/tg1-5. Accessed 26 Sep 2024

632 24. Marini G, Rosá R, Pugliese A, Heesterbeek H (2017) Exploring vector-borne infection
633 ecology in multi-host communities: A case study of West Nile virus. J Theor Biol
634 415:58–69

635 25. Simpson JE, Hurtado PJ, Medlock J, Molaei G, Andreadis TG, Galvani AP, Diuk-Wasser
636 MA (2012) Vector host-feeding preferences drive transmission of multi-host
637 pathogens: West Nile virus as a model system. Proc Biol Sci 279:925–933

638 26. Cruz-Pacheco G, Esteva L, Vargas C (2012) Multi-species interactions in West Nile virus
639 infection. J Biol Dyn 6:281–298

640 27. Robertson SL, Caillouët KA (2016) A host stage-structured model of enzootic West Nile
641 virus transmission to explore the effect of avian stage-dependent exposure to vectors.
642 J Theor Biol 399:33–42

643 28. Maidana NA, Yang HM (2011) Dynamic of West Nile Virus transmission considering
644 several coexisting avian populations. Math Comput Model 53:1247–1260

645 29. Beebe TA, Robertson SL (2017) A two-species stage-structured model for West Nile
646 virus transmission. Lett Biomath 4:112–132

647 30. Blom R, Krol L, Langezaal M, Schrama M, Trimbos KB, Wassenaar D, Koenraadt CJM
648 (2024) Blood-feeding patterns of Culex pipiens biotype pipiens and pipiens/molestus
649 hybrids in relation to avian community composition in urban habitats. Parasit Vectors
650 17:1–12

651 31. Rizzoli A, Bolzoni L, Chadwick EA, et al (2015) Understanding West Nile virus ecology in
652 Europe: Culex pipiens host feeding preference in a hotspot of virus emergence. Parasit
653 Vectors. https://doi.org/10.1186/s13071-015-0831-4

654 32. Meister T, Lussy H, Bakonyi T, et al (2008) Serological evidence of continuing high
655 Usutu virus (Flaviviridae) activity and establishment of herd immunity in wild birds in
656 Austria. Vet Microbiol 127:237–248

657 33. Magallanes S, Llorente F, Ruiz-López MJ, et al (2024) Warm winters are associated to
658 more intense West Nile virus circulation in southern Spain. Emerg Microbes Infect.
659 https://doi.org/10.1080/22221751.2024.2348510

660 34. Escribano-Romero E, Jiménez de Oya N, Camacho MC, Blázquez AB, Martín-Acebes
661 MA, Risalde MA, Muriel L, Saiz JC, Höfle U (2021) Previous Usutu Virus Exposure
662 Partially Protects Magpies (Pica pica) against West Nile Virus Disease But Does Not
663 Prevent Horizontal Transmission. Viruses. https://doi.org/10.3390/V13071409

664 35. Magpie | BTO - British Trust for Ornithology. https://www.bto.org/understanding-
665 birds/birdfacts/magpie. Accessed 8 May 2024

666 36. Coombs CFB, Isaacson AJ, Murton RK, Thearle RJP, Westwood NJ (1981) Collared Doves
667 (Streptopelia decaocto) in Urban Habitats. J Appl Ecol 18:41

668 37. Yaremych SA, Novak RJ, Raim AJ, Mankin PC, Warner RE (2004) HOME RANGE AND
669 HABITAT USE BY AMERICAN CROWS IN RELATION TO TRANSMISSION OF WEST NILE
670 VIRUS. https://doi.org/101676/03-104 116:232–239

671 38. Cadar D, Lühken R, van der Jeugd H, et al (2017) Widespread activity of multiple
672 lineages of Usutu virus, Western Europe, 2016. Eurosurveillance.
673 https://doi.org/10.2807/1560-7917.ES.2017.22.4.30452

674 39. Sieg M, Schmidt V, Ziegler U, et al (2017) Outbreak and Cocirculation of Three Different
675 Usutu Virus Strains in Eastern Germany. Vector-Borne and Zoonotic Diseases 17:662–
676 664

677 40. Young JJ, Haussig JM, Aberle SW, Pervanidou D, Riccardo F, Sekulić N, Bakonyi T,
678 Gossner CM (2021) Epidemiology of human West Nile virus infections in the European
679 Union and European Union enlargement countries, 2010 to 2018. Eurosurveillance
680 26:2001095

681 41. Visser ME, Both C, Lambrechts MM (2004) Global Climate Change Leads to Mistimed
682 Avian Reproduction. Adv Ecol Res 35:89–110

683 42. Sauer FG, Timmermann E, Lange U, Lühken R, Kiel E (2022) Effects of Hibernation Site,
684 Temperature, and Humidity on the Abundance and Survival of Overwintering Culex
685 pipiens pipiens and Anopheles messeae (Diptera: Culicidae). J Med Entomol 59:2013–
686 2021

687 43. De Angelis D, Presanis AM, Birrell PJ, Tomba GS, House T (2015) Four key challenges in
688 infectious disease modelling using data from multiple sources. Epidemics 10:83–87

689 44. Wonham MJ, De-Camino-Beck T, Lewis MA (2004) An epidemiological model for West
690 Nile virus: Invasion analysis and control applications. Proceedings of the Royal Society
691 B: Biological Sciences 271:501–507

692 45. Anderson RM, May RM (1991) Infectious Diseases of Humans: Dynamics and Control.
693 OUP Oxford

694 46. Paradis E, Baillie SR, Sutherland WJ, Gregory RD (1998) Patterns of natal and breeding
695 dispersal in birds. Journal of Animal Ecology 67:518–536

47. Boulinier T, Kada S, Ponchon A, et al (2016) Migration, Prospecting, Dispersal? What Host Movement Matters for Infectious Agent Circulation? Integr Comp Biol 56:330–342

48. Van Vliet J, Musters CJM, Ter Keurs WJ (2009) Changes in migration behaviour of Blackbirds Turdus merula from the Netherlands. Bird Study 56:276–281

49. Hamer GL, Anderson TK, Donovan DJ, et al (2014) Dispersal of Adult Culex Mosquitoes in an Urban West Nile Virus Hotspot: A Mark-Capture Study Incorporating Stable Isotope Enrichment of Natural Larval Habitats. PLoS Negl Trop Dis 8:e2768

50. Schoppers J, van Turnhout C, van Diek H (2020) Handleiding Meetnet Urbane Soorten (MUS). .

51. Teunissen WA, Wiersma P, de Jong A, Kleyheeg E, Vergeer J-W (2019) Handleiding voor het Meetnet Agrarische Soorten. .

52. Vergeer JW, Boele A, van Bruggen J, van Turnhout C (2023) Handleiding Sovon Broedvogelmonitoring: Broedvogel Monitoring Project en kolonievogels. Sovon Vogelonderzoek Nederland, Nijmegen

53. Vigie-Nature. (2021) Base de données du Suivi Temporel des Oiseaux Communs / Common Bird Monitoring Scheme database for France.

54. Ibañez-Justicia A, Stroo A, Dik M, Beeuwkes J, Scholte EJ (2015) National mosquito (Diptera: Culicidae) survey in the Netherlands 2010-2013. J Med Entomol 52:185–198

55. Bortel W Van, Versteirt V, Dekoninck W, Hance T, Brosens D, Hendrickx G (2022) MODIRISK: Mosquito vectors of disease, collection, monitoring and longitudinal data from Belgium. GigaByte 2022:gigabyte58

56. Beaunée G (2024) Batched Resilient and Rapid Estimation Workflow through Approximate Bayesian Computation. R package version 1.0.0. https://github.com/GaelBn/BRREWABC/.

57. Sisson SA, Fan Y, Tanaka MM (2007) Sequential Monte Carlo without likelihoods. Proc Natl Acad Sci U S A 104:1760–1765

58. Toni T, Welch D, Strelkowa N, Ipsen A, Stumpf MPH (2008) Approximate Bayesian computation scheme for parameter inference and model selection in dynamical systems. J R Soc Interface 6:187–202

59. Diekmann O, Heesterbeek JAP, Roberts MG (2010) The construction of next-generation matrices for compartmental epidemic models. J R Soc Interface 7:873–885

60. Boele A, Vergeer J, Van Bruggen J, et al (2023) Broedvogels in Nederland in 2022. Sovon-rapport 2023/40.

61. Birdfact (2023) Blackbird Nesting: A Complete Guide | Birdfact. In: Birdfact.com. https://birdfact.com/articles/blackbird-nesting. Accessed 7 Dec 2023

62. van den Bremer L, van Turnhout C (2021) Voorstudie Jaar van de Merel 2022. Sovon-rapport 2021/56. Nijmegen

63. Robinson RA, Kew JJ, Kew AJ (2010) Survival of suburban blackbirds Turdus merula varies seasonally but not by sex. J Avian Biol 41:83–87

64. Ewing DA, Cobbold CA, Purse B V., Nunn MA, White SM (2016) Modelling the effect of temperature on the seasonal population dynamics of temperate mosquitoes. J Theor Biol 400:65–79

65. UK: average temperature by month 2023 | Statista. https://www.statista.com/statistics/322658/monthly-average-daily-temperatures-in-the-united-kingdom-uk/. Accessed 2 May 2024

66. KNMI - Maandgemiddelde temperaturen, normalen, anomalieën. https://www.knmi.nl/nederland-nu/klimatologie/geografische-overzichten/archief/maand/tg. Accessed 2 May 2024

67. Perkins TA, Reiner RC, España G, et al (2019) An agent-based model of dengue virus transmission shows how uncertainty about breakthrough infections influences vaccination impact projections. PLoS Comput Biol 15:e1006710

68. Kuchinsky SC, Marano J, Hawks SA, Loessberg E, Honaker CF, Siegel PB, Lahondère C, LeRoith T, Weger-Lucarelli J, Duggal NK (2022) North American House Sparrows Are Competent for Usutu Virus Transmission. mSphere. https://doi.org/10.1128/MSPHERE.00295-22

69. Rubel F, Brugger K, Hantel M, Chvala-Mannsberger S, Bakonyi T, Weissenböck H, Nowotny N (2008) Explaining Usutu virus dynamics in Austria: Model development and calibration. Prev Vet Med 85:166–186

70. Nicholas Komar (2003) West Nile Virus: Epidemiology and Ecology in North America. pp 185–234

71. McKee EM, Walker ED, Anderson TK, et al (2015) WEST NILE VIRUS ANTIBODY DECAY RATE IN FREE-RANGING BIRDS. J Wildl Dis 51:601–608

72. Shocket MS, Verwillow AB, Numazu MG, Slamani H, Cohen JM, El Moustaid F, Rohr J, Johnson LR, Mordecai EA (2020) Transmission of west nile and five other temperate mosquito-borne viruses peaks at temperatures between 23˚C and 26˚C. Elife 9:1–67

73. Ciota AT, Matacchiero AC, Kilpatrick AM, Kramer LD (2014) The Effect of Temperature on Life History Traits of Culex Mosquitoes. J Med Entomol 51:55–62

74. Ruybal JE, Kramer LD, Kilpatrick AM (2016) Geographic variation in the response of Culex pipiens life history traits to temperature. Parasit Vectors 9:116

75. Andreadis SS, Dimotsiou OC, Savopoulou-Soultani M (2014) Variation in adult longevity of Culex pipiens f. pipiens, vector of the West Nile Virus. Parasitol Res 113:4315–4319

76. Reisen WK, Fang Y, Martinez VM (2006) Effects of Temperature on the Transmission of West Nile Virus by Culex tarsalis (Diptera: Culicidae). J Med Entomol 43:309–317

77. Dohm DJ, Sardelis MR, Turell MJ (2002) Experimental Vertical Transmission of West Nile Virus by Culex pipiens (Diptera: Culicidae). J Med Entomol 39:640–644

78. Kilpatrick AM, Meola MA, Moudy RM, Kramer LD (2008) Temperature, viral genetics, and the transmission of West Nile virus by Culex pipiens mosquitoes. PLoS Pathog. https://doi.org/10.1371/JOURNAL.PPAT.1000092

79. Field EN, Shepard JJ, Clifton ME, et al (2022) Semi-field and surveillance data define the natural diapause timeline for Culex pipiens across the United States. Communications Biology 2022 5:1 5:1–12

80. Widgren S, Bauer P, Eriksson R, Engblom S (2019) Siminf: An R package for data-driven stochastic disease spread simulations. J Stat Softw 91:1–42

81. Davis BE (2007) Habitat use, movements, and survival of radio-marked female mallards in the lower Mississippi Alluvial Valley. LSU Master's Theses. https://doi.org/10.31390/gradschool_theses.215

82. de Bellegarde de Saint Lary C, Kasbergen LMR, Bruijning-Verhagen PCJL, et al (2023) Assessing West Nile virus (WNV) and Usutu virus (USUV) exposure in bird ringers in the Netherlands: a high-risk group for WNV and USUV infection? One Health 16:100533

83. Cleton NB, Godeke GJ, Reimerink J, et al (2015) Spot the Difference—Development of a Syndrome Based Protein Microarray for Specific Serological Detection of Multiple Flavivirus Infections in Travelers. PLoS Negl Trop Dis 9:e0003580

84. Dutch Wildlife Health Centre (DWHC) & Sovon (2023) Dode vogels melden. In: https://dwhc.nl/publicaties/#informatie-en-downloads.

85. Del Moral P, Doucet A, Jasra A (2006) Sequential Monte Carlo samplers. J R Stat Soc Series B Stat Methodol 68:411–436

86. Del Moral P, Doucet A, Jasra A (2012) An adaptive sequential Monte Carlo method for approximate Bayesian computation. Stat Comput 22:1009–1020

87. Drovandi CC, Pettitt AN (2011) Estimation of Parameters for Macroparasite Population Evolution Using Approximate Bayesian Computation. Biometrics 67:225–233

88. Beaumont MA, Cornuet JM, Marin JM, Robert CP (2009) Adaptive approximate Bayesian computation. Biometrika 96:983–990

89. Adams B, Boots M (2010) How important is vertical transmission in mosquitoes for the persistence of dengue? Insights from a mathematical model. Epidemics 2:1–10

90. Turell MJ, O'Guinn ML, Dohm DJ, Jones JW (2001) Vector competence of North American mosquitoes (Diptera: Culicidae) for West Nile virus. J Med Entomol 38:130–134

Supplementary materials

- Supplementary Material A: Model formulation and parameterisation
- Supplementary Material B: Bird dispersal
- Supplementary Material C: Surveillance data
- Supplementary Material D: Inference approach
- Supplementary Material E: Validation of inference approach
- Supplementary Material F: Additional results
- Supplementary Material G: Inference diagnostics
- Supplementary Material H: Reproduction numbers

Supplementary Material A: Model formulation and parameterisation

The equations for the modelled system (Eq 1-23) describe susceptible (Sm), exposed (Em), and infectious (Im) mosquitoes, where the total adult mosquito population is Nm = Sm + Em + Im, and susceptible (S), exposed (E), infectious (I), recovered (R) and dead (D) birds. The bird population is split into two groups: reservoir birds and blackbirds, which are further split into two age classes: those under 1 year old (juvenile blackbirds (*JB)* and juvenile reservoir birds (*JR*)) and those above 1 year of age (adult blackbirds (*AB)* and adult reservoir birds (*AR*)). For each group, the total live bird population in grid cell *i* is N*i* = S*i* + E*i* + I*i* + R*i*.

Mosquito population:

$$\frac{d\,S_{M,i}}{dt} = \delta_M(t) * N_{M,i} - b(T) * q * p_{MB} * S_{M,i} * \left(\frac{N_{JB,i}}{(N_{JR,i}+N_{AR,i})*\,\omega+N_{JB,i}+N_{AB,i}} * \frac{fb_{ii}*I_{JB,i}+\sum_j fb_{ji}*I_{JB,j}}{fb_{ii}*N_{JB,i}+\sum_j fb_{ji}*N_{JB,j}} + \frac{N_{AB,i}}{(N_{JR,i}+N_{AR,i})*\,\omega+N_{JB,i}+N_{AB,i}} * \frac{fb_{ii}*I_{AB,i}+\sum_j fb_{ji}*I_{AB,j}}{fb_{ii}*N_{AB,i}+\sum_j fb_{ji}*N_{AB,j}} + \frac{N_{JR,i}*\,\omega}{(N_{JR,i}+N_{AR,i})*\,\omega+N_{JB,i}+N_{AB,i}} * \frac{fr_{ii}*I_{JR,i}+\sum_j fr_{ji}*I_{JR,j}}{fr_{ii}*N_{JR,i}+\sum_j fr_{ji}*N_{JR,j}} + \frac{N_{AR,i}*\,\omega}{(N_{JR,i}+N_{AR,i})*\,\omega+N_{JB,i}+N_{AB,i}} * \frac{fr_{ii}*I_{AR,i}+\sum_j fr_{ji}*I_{AR,j}}{fr_{ii}*N_{AR,i}+\sum_j fr_{ji}*N_{AR,j}}\right) - \mu_M(T) * S_{M,i} - \sigma(t) * S_{M,i} \quad (1)$$

$$\frac{d\,E_{M,i}}{dt} = b(T) * q * p_{MB} * S_{M,i} * \left(\frac{N_{JB,i}}{(N_{JR,i}+N_{AR,i})*\,\omega+N_{JB,i}+N_{AB,i}} * \frac{fb_{ii}*I_{JB,i}+\sum_j fb_{ji}*I_{JB,j}}{fb_{ii}*N_{JB,i}+\sum_j fb_{ji}*N_{JB,j}} + \frac{N_{AB,i}}{(N_{JR,i}+N_{AR,i})*\,\omega+N_{JB,i}+N_{AB,i}} * \frac{fb_{ii}*I_{AB,i}+\sum_j fb_{ji}*I_{AB,j}}{fb_{ii}*N_{AB,i}+\sum_j fb_{ji}*N_{AB,j}} + \frac{N_{JR,i}*\,\omega}{(N_{JR,i}+N_{AR,i})*\,\omega+N_{JB,i}+N_{AB,i}} * \frac{fr_{ii}*I_{JR,i}+\sum_j fr_{ji}*I_{JR,j}}{fr_{ii}*N_{JR,i}+\sum_j fr_{ji}*N_{JR,j}} + \frac{N_{AR,i}*\,\omega}{(N_{JR,i}+N_{AR,i})*\,\omega+N_{JB,i}+N_{AB,i}} ** \frac{fr_{ii}*I_{AR,i}+\sum_j fr_{ji}*I_{AR,j}}{fr_{ii}*N_{AR,i}+\sum_j fr_{ji}*N_{AR,j}}\right) - u(T) * E_{M,i} - \mu_M(T) * E_{M,i} - \sigma(t) * E_{M,i} \quad (2)$$

$$\frac{d\,I_{M,i}}{dt} = u(T) * E_{M,i} - \mu_M(T) * I_{M,i} - \sigma(t) * I_{M,i} \quad (3)$$

Juvenile blackbird population:

$$\frac{d\,S_{JB,i}}{dt} = \delta_B(t) + \rho * R_{JB,i} - b(T) * q * p_{BM} * S_{JB,i} * \left(\frac{N_{JB,i}}{(N_{JR,i}+N_{AR,i})*\,\omega+N_{JB,i}+N_{AB,i}} * \frac{fb_{ii}*I_{M,i}+\sum_j fb_{ji}*I_{M,j}}{fb_{ii}*N_{JB,i}+\sum_j fb_{ji}*N_{JB,j}}\right) - \mu_{JB} * S_{JB,i} \quad (4)$$

$$\frac{d\,E_{JB,i}}{dt} = b(T) * q * p_{BM} * S_{JB,i} * \left(\frac{N_{JB,i}}{(N_{JR,i}+N_{AR,i})*\,\omega+N_{JB,i}+N_{AB,i}} * \frac{fb_{ii}*I_{M,i}+\sum_j fb_{ji}*I_{M,j}}{fb_{ii}*N_{JB,i}+\sum_j fb_{ji}*N_{JB,j}}\right) - \varepsilon * E_{JB,i} - \mu_{JB} * E_{JB,i} \quad (5)$$

$$\frac{d\,I_{JB,i}}{dt} = \varepsilon * E_{JB,i} - \gamma * I_{JB,i} - \mu_{JB} * I_{JB,i} - v * I_{JB,i} \quad (6)$$

$$\frac{d\,R_{JB,i}}{dt} = \gamma * I_{JB,i} - \mu_{JB} * R_{JB,i} - \rho * R_{JB,i} \quad (7)$$

$$\frac{d\,D_{JB,i}}{dt} = \mu_{JB} * \left(S_{JB,i} + E_{JB,i} + I_{JB,i} + R_{JB,i}\right) + v * I_{JB,i} \quad (8)$$

Adult blackbird population:

$$\frac{d\,S_{AB,i}}{dt} = a_{JB} * S_{JB,i} + \rho * R_{AB,i} - b(T) * q * p_{BM} * S_{AB,i} * \left(\frac{N_{AB,i}}{(N_{JR,i}+N_{AR,i}) * \omega + N_{JB,i} + N_{AB,i}} * \frac{fb_{ii} * I_{M,i} + \sum_j fb_{ji} * I_{M,j}}{fb_{ii} * N_{AB,i} + \sum_j fb_{ji} * N_{AB,j}}\right) - \mu_{AB} * S_{AB,i} \quad (9)$$

$$\frac{d\,E_{AB,i}}{dt} = a * E_{JB,i} + b(T) * q * p_{BM} * S_{AB,i} * \left(\frac{N_{AB,i}}{(N_{JR,i}+N_{AR,i}) * \omega + N_{JB,i} + N_{AB,i}} * \frac{fb_{ii} * I_{M,i} + \sum_j fb_{ji} * I_{M,j}}{fb_{ii} * N_{AB,i} + \sum_j fb_{ji} * N_{AB,j}}\right) - \varepsilon * E_{AB,i} - \mu_{AB} * E_{AB,i} \quad (10)$$

$$\frac{d\,I_{AB,i}}{dt} = a * I_{JB,i} + \varepsilon * E_{AB,i} - \gamma * I_{AB,i} - \mu_{AB} * I_{AB,i} - v * I_{AB,i} \quad (11)$$

$$\frac{d\,R_{AB,i}}{dt} = a * R_{JB,i} + \gamma * I_{AB,i} - \mu_{AB} * R_{AB,i} - \rho * R_{AB,i} \quad (12)$$

$$\frac{d\,D_{AB,i}}{dt} = \mu_{AB} * \left(S_{AB,i} + E_{AB,i} + I_{AB,i} + R_{AB,i}\right) + v * I_{AB,i} \quad (13)$$

Juvenile reservoir population:

$$\frac{d\,S_{JR,i}}{dt} = \rho * R_{JR,i} - b(T) * q * p_{BM} * S_{JR,i} * \left(\frac{N_{JR,i} * \omega}{(N_{JR,i}+N_{AR,i}) * \omega + N_{JB,i} + N_{AB,i}} * \frac{fr_{ii} * I_{M,i} + \sum_j fr_{ji} * I_{M,j}}{fr_{ii} * N_{JR,i} + \sum_j fr_{ji} * N_{JR,j}}\right) - \mu_{JR} * S_{JR,i} \quad (14)$$

$$\frac{d\,E_{JR,i}}{dt} = b(T) * q * p_{BM} * S_{JR,i} * \left(\frac{N_{JR,i} * \omega}{(N_{JR,i}+N_{AR,i}) * \omega + N_{JB,i} + N_{AB,i}} * \frac{fr_{ii} * I_{M,i} + \sum_j fr_{ji} * I_{M,j}}{fr_{ii} * N_{JR,i} + \sum_j fr_{ji} * N_{JR,j}}\right) - \varepsilon * E_{JR,i} - \mu_{JR} * E_{JR,i} \quad (15)$$

$$\frac{d\,I_{JR,i}}{dt} = \varepsilon * E_{JR,i} - \gamma * I_{JR,i} - \mu_{JR} * I_{JR,i} \quad (16)$$

$$\frac{d\,R_{JR,i}}{dt} = \gamma * I_{JR,i} - \mu_{JR} * R_{JR,i} - \rho * R_{JR,i} \quad (17)$$

$$\frac{d\,D_{JR,i}}{dt} = \mu_{JR} * \left(S_{JR,i} + E_{JR,i} + I_{JR,i} + R_{JR,i}\right) \quad (18)$$

Adult reservoir population:

$$\frac{d\,S_{AR,i}}{dt} = a_{JR} * S_{JR,i} + \rho * R_{AR,i} - b(T) * q * p_{BM} * S_{AR,i} * \left(\frac{N_{AR,i} * \omega}{(N_{JR,i}+N_{AR,i}) * \omega + N_{JB,i} + N_{AB,i}} * \frac{fr_{ii} * I_{M,i} + \sum_j fr_{ji} * I_{M,j}}{fr_{ii} * N_{AR,i} + \sum_j fr_{ji} * N_{AR,j}}\right) - \mu_{AR} * S_{AR,i} \quad (19)$$

$$\frac{d\,E_{AR,i}}{dt} = b(T) * q * p_{BM} * S_{AR,i} * \left(\frac{N_{AR,i} * \omega}{(N_{JR,i}+N_{AR,i}) * \omega + N_{JB,i} + N_{AB,i}} * \frac{fr_{ii} * I_{M,i} + \sum_j fr_{ji} * I_{M,j}}{fr_{ii} * N_{AR,i} + \sum_j fr_{ji} * N_{AR,j}}\right) - \varepsilon * E_{AR,i} - \mu_{JR} * E_{AR,i} \quad (20)$$

$$\frac{d\,I_{AR,i}}{dt} = \varepsilon * E_{AR,i} - \gamma * I_{AR,i} - \mu_{AR} * I_{AR,i} \quad (21)$$

$$\frac{d\,R_{AR,i}}{dt} = \gamma * I_{AR,i} - \mu_{AR} * R_{AR,i} - \rho * R_{AR,i} \quad (22)$$

$$\frac{d\,D_{AR,i}}{dt} = \mu_{AR} * \left(S_{AR,i} + E_{AR,i} + I_{AR,i} + R_{AR,i}\right) \quad (23)$$

Model parameters

Parameter values are described in Table 2. These can be time-dependent (t) or temperature-dependent (T). Most model parameters were directly obtained from literature, however some were based on calculations.

<u>Proportion of bites on competent hosts</u>

As *Culex pipiens/torrentium* mosquitoes bite a wide range of hosts [30], we accounted for the presence of non-competent hosts. For this, we used a parameter that determines the proportion of mosquito bites that are on competent hosts and assumed that the modelled bird populations represent all competent hosts. We also assumed that the total number of (competent and non-competent) hosts is the same in each location. The proportion of bites that are on competent hosts was set equal to the proportion of the total bird population that are competent. This proportion was calculated each day and location, by setting it to 100% in the location where the bird population density was largest. In all other locations this proportion was equivalent to the relative density compared to the cell where this was largest.

<u>Bird birth rate</u>

The bird death rate was assumed to be constant over space and time, while births occurred seasonally. These births were distributed uniformly across the period where newborns start leaving their nests assuming a hatching period of 14 days and a further 14 days until they fledge the nest [56]. Ageing from juvenile to adult bird occurred instantaneously on the last day of April, the day before births start.

We used a Leslie matrix to calculate the annual number of births assuming the population remains constant in absence of infection. The following Leslie matrix was developed for the blackbird population, where F stands for the annual fertility rate and S for the annual survival rate of juvenile (j) or adult (a) birds:

$$A = \begin{matrix} Fj & Fa \\ Sj & Sa \end{matrix} = \begin{matrix} 0 & Fa \\ 0.13 & 0.68 \end{matrix}$$

We calculated the fertility rate for adults for which the eigenvalue of the matrix equals 1. The resulting fertility rate was 2.5 births per year, using juvenile survival estimates from [57] and adult survival estimates from [58]. While the blackbird population declined during the first three years of USUV circulation, the population recovered in subsequent years. In the model, we included the possibility of population recovery by assuming a fixed number of annual births (i.e. independent of the population size.) Therefore we calculated the daily number of births during the breeding period based on the population size at the beginning of 2016 (2.5 births / 45 days = 0.056 births per bird per day) and used this fixed value for all years.

Annual survival probabilities were transformed to daily mortality rates to be used in the simulation model based on the following equation: $annual\ survival\ probability = (1 - daily\ mortality\ rate)$^365.

The same approach was used for the modelled reservoir population. When the adult lifespan was a parameter to be estimated (in models C, D, S1, S2, S3), the calculations were performed for each simulation run.

Diapause

The proportion of active adult mosquitoes ($\vartheta(t)$) is dependent on daylength $\varphi(t)$ and temperature:

$$\vartheta(t) = \frac{1}{1+\exp\left(5\left(\delta_A - \varphi(t)\right)\right)},$$

where δ_A is the autumn threshold when the mosquito population starts entering diapause [59]. While estimates of the autumn threshold value are lacking for the Netherlands, this value was estimated to be 13 in the United Kingdom [59]. Using this threshold with local estimates of daylength suggests that that mosquitoes start entering diapause around the beginning of September and all mosquitoes are in diapause towards the end of September. To adjust for somewhat warmer autumn temperatures in the Netherlands compared to the United Kingdom [60,61] and to match observations from local mosquito trapping data, we assumed that the average time to entering diapause (since 1st September) was 20 days, leading to an estimated rate of 0.05 at which mosquitoes enter diapause. In our model, mosquitoes entered diapause in the period between September to mid-October at this fixed daily rate. Any remaining active mosquitoes at the end of this period were forced to enter diapause in mid-October. Mosquitoes re-emerged from diapause on the first of April, following estimates from the abundance model.

Virus re-emergence

The re-emergence of USUV after winter was included in the model through reseeding infections in mosquitoes on the second of April each year (the day after mosquitoes re-emerged from diapause). This was implemented as an infection rate moving mosquitoes from the susceptible to exposed state. This rate was determined for each location separately by multiplying the prevalence in mosquitoes at the end of the previous season in each location (in mid-September) by the re-emergence rate parameter. The value of this parameter was estimated during model calibration and was the same across all locations and years. Re-emergence of USUV in spring represents the possibility of local overwintering and/or re-introductions from migratory birds.

Host-vector abundance scaling parameter

Bird and mosquito abundance estimates were on a relative scale, because the total population size is not known for these populations. We therefore introduced a host-vector abundance scaling parameter, which converts the host and vector abundance to be on the same scale, meaning that their ratio reflects the vector-to-host ratio. This parameter was used to determine the initial conditions of the model and was therefore not included in the differential equations.

Mosquito emergence and death rate

Mosquito abundance estimates were used to estimate vital dynamics in the mosquito population. Mosquito death rate was assumed temperature-dependent (Supplementary Material Table 2) and therefore differed over space and time. Similar to Perkins et al. [67], the number of emerging mosquitoes was estimated for each location and day such that, together with the mortality rates, the resulting population size follows estimates from the abundance model.

Table 2: Parameters and their values used in the model. T indicates temperature, t indicates time.

Parameter	Description	Value	Source
Blackbirds			
$\delta_b(t)$	Daily number of births	1 May – 15 June: 0.056 per bird Else: 0	Value: calculated, see above. Timing: [57]
μ_{JB}	Mortality rate, juvenile	0.0059 / day	[57]

μ_{AB}	Mortality rate, adult	0.0011 / day	[58]
p_{bm}	Transmission probability, mosquito to blackbird	0.88	[44]
ε	Intrinsic incubation rate	0.67 / day	[63,64]
γ	Recovery rate	0.25 / day	[65]
v	Disease-induced mortality rate	NA	To be estimated
ρ	Rate of immunity loss	0.0014 / day	[66]
fb_{ji}	Fraction of blackbirds in cell *j* dispersing to *i*	Variable	Calculated, see Supplementary Material B
a_{JB}	Ageing rate from juvenile to adult	On 30th April: 1. Else: 0	[57]
Additional reservoir population			
$\delta_r(t)$	Daily number of births	1 May – 15 June: To be estimated Else: 0	Value: to be estimated. See above. Timing: [57]
μ_{JR}	Mortality rate, juvenile	0.0059 / day	Set equal to blackbird juvenile
μ_{AR}	Mortality rate, adult	NA	To be estimated
p_{bm}	Transmission probability, mosquito to reservoir host	0.88	[44]
ε	Intrinsic incubation rate	0.67 / day	[63,64]
γ	Recovery rate	0.25 / day	[65]
ρ	Rate of immunity loss	0.0014 / day	[66]
fr_{ji}	Fraction of reservoir birds in cell *j* dispersing to *i*	Variable	Calculated, see Supplementary Material B
a_{JR}	Ageing rate from juvenile to adult	On 30th April: 1. Else: 0	Set equal to blackbird
ω	Relative biting frequency	NA	To be estimated
Culex pipiens			
$\delta_m(t)$	Emergence rate	Variable	Estimated from abundance data, see above
$\mu_m(T)$	Mortality rate [daily]	For T<33 °C: 1 / (-4.86*T + 169.8), else 0.17	[67] fitted to data from [68–70]
b(T)	Biting rate [daily]	0.344/(1+1.231*exp(-0.184*(T-20)))	[64] fitted to data from [71]
q	Proportion of bites that are on competent host	Variable	Calculated, see above
p_{mb}	Transmission probability, blackbird & reservoir population to mosquito	NA	To be estimated
u(T)	Extrinsic incubation rate [daily]	For T>13 °C: $7.38*10^{-5} * T * (T – 11.4)(45.2 – T)^{1/2}$, else 0	[67] fitted to data from [72,73]
σ(t)	Rate of entering diapause	1 Sept – 15 Oct: 0.05. Else: 0	[74]

Model design and implementation

The model was implemented using the SimInf package [80]. The model consisted of both stochastic and deterministic processes. The majority of processes (including transitions between compartments and daily dispersal) are modelled as continuous-time discrete variable Markov chains using the direct Gillespie stochastic simulation algorithm. Bird birth events were processed deterministically (and are therefore not shown in the model equations) to ensure an equal number of births each year, independent of changes in the population size due to virus transmission. This allowed for the recovery of the host population size after increased death rates due to infection. Mosquito emergence and death rates were also processed deterministically, to ensure the mosquito population sizes always follow the predicted abundance (see 'Input layers'). Seasonal movements of birds were also included deterministically. These deterministic processes are executed at the end of each time step for which they were planned.

Overview of data inputs

Information on blackbird abundance, *Cx. pipiens* abundance and temperature was obtained from literature, see main text. Supplementary Figure 5 provides an overview of these input data.

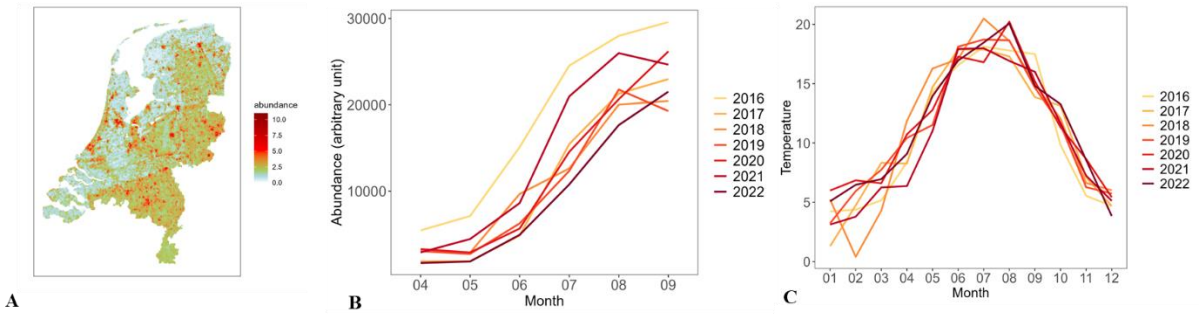

Supplementary Figure 5: A. Relative blackbird abundance map. B. Monthly estimates of the relative abundance of Culex pipiens mosquitoes in the Netherlands for each year. C. Mean monthly temperature during 2016-2022.

Supplementary Material B: Bird dispersal

The Vogeltrekstation NIOO-KNAW dataset containing Dutch ringing recovery information was used to estimate bird movement distances. We created a dataset (n=333) using the following criteria:

- Blackbirds
- Observations from 1970 onwards
- Two observations per bird available: ringing and dead recovery (at least one day later)
- Ringed and recovered within the Netherlands
- High accuracy in location, age and date information
- Ringed in breeding season (April, May, June) or post-breeding season (July, August, September)
- Juvenile or adult stage (nestlings were excluded, because they cannot move)

The final dataset included observations from all provinces, although most observations came from the North and Middle regions (Supplementary figure 6).

Two movement patterns were distinguished in the model, representing daily movements and seasonal dispersal. Daily movements include foraging-type movements often within the bird's home range, i.e. the area the bird regularly traverses around in its territory. In addition to daily movements, we included seasonal dispersal that represents the search for a new nest location. Seasonal dispersal takes place during the change from breeding to post-breeding season in early July.

To parameterize these processes, we compared distance between ringing and recovery location within seasons (daily movements) and between breeding and subsequent seasons (seasonal dispersal). Only bird movement during the transmission season was included, which was divided into two periods: breeding season (April to July) and post-breeding season (July to October). The bird population was divided into two age groups: juvenile (from fledging until the next breeding season) and adult (birds older than one year).

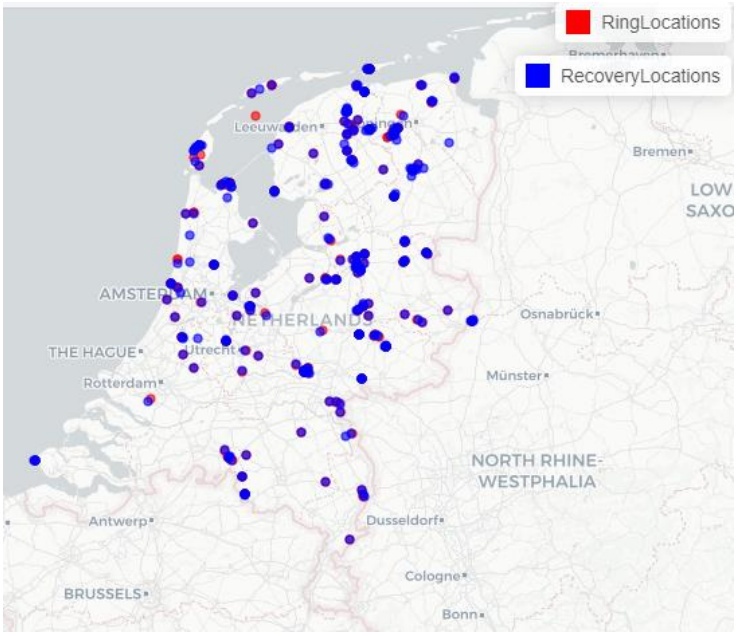

Supplementary figure 6: Locations of ringed and recovered birds

Daily movements

We found no evidence of an association between distance and days since ringing (p=0.30) (Supplementary figure 7). For blackbirds that were ringed and recovered in the same season of the

same year, we therefore assumed that the distance between ringing and recovery location represents the daily movement distance around the home base.

No difference was found in daily movement distance between juvenile and adult blackbirds (Wilcoxon rank sum test breeding season: p=0.51 & post-breeding season: p=0.52). However, there was evidence for a difference in movement distances between breeding and post-breeding season (Wilcoxon rank sum test p=0.03, Supplementary figure 8). We therefore estimated daily movement for each season, combining both age groups.

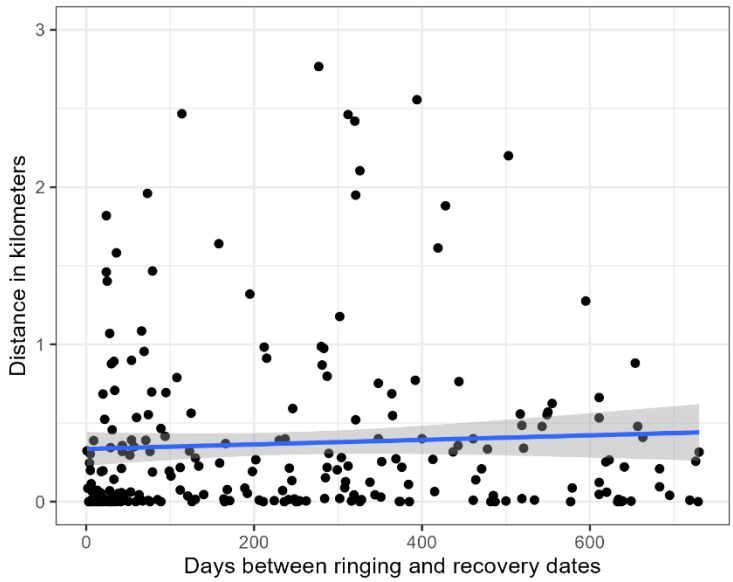

Supplementary figure 7: Relationship between distance and days since ringing.

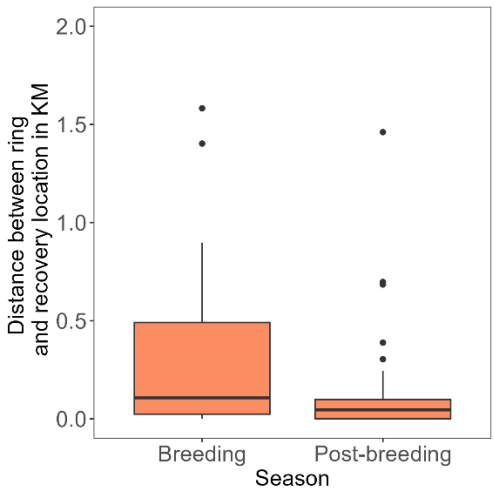

Supplementary figure 8: Distance between ring and recovery location of blackbirds by season. Only blackbirds ringed and recovered within the same season were included.

We fitted Weibull, gamma, and exponential distributions to each dataset and compared fits based on AIC (Supplementary table 3). The fitting of an exponential distribution was not possible for breeding season due to extreme outliers. As the Weibull distribution was the best fitting distribution in both cases, we used parameters from this distribution to calculate daily movement matrices. This resulted in a median daily movement distance of 143 m (inter-quartile range 19 - 692) during breeding season and 29 m (inter-quartile range 4 – 129) during post-breeding season.

Supplementary table 3: AIC values of three different distributions fitted to within-season dispersal distance and parameter estimates of the fitted Weibull distributions.

	Weibull	Gamma	Exponential		
				Weibull parameters	
				Scale	Shape
Breeding (n=23)	324	330	NA	329.4	0.44
Post-breeding (n=31)	331	333	375	63.4	0.46

Seasonal dispersal

The same approach was used to quantify between-season dispersal. To estimate the distance blackbirds move during seasonal dispersal, we selected birds that were ringed in breeding season and recovered after this season. There was evidence for a difference in seasonal dispersal distances between adult and juvenile birds (Wilcoxon rank sum test p=0.04), see Supplementary figure 9. In the transmission simulation model, seasonal dispersal took place once a year on the change from breeding to post-breeding season (1st of July).

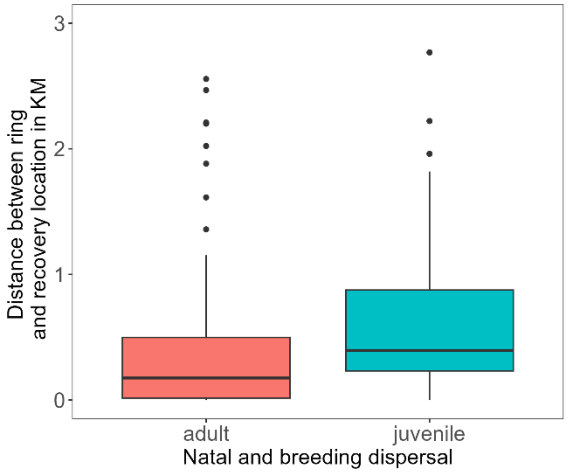

Supplementary figure 9: Distance between ringing and recovery location of blackbirds by age for birds ringed during breeding season and recovered after this season.

Again, we fitted Weibull, gamma, and exponential distributions to each dataset and compared fits based on AIC (Supplementary table 4). The fitting of an exponential distribution was not possible for both datasets due to extreme outliers. As the Weibull distribution was the best fitting distribution on average, we used parameters from this distribution (Supplementary table 4) to calculate seasonal dispersal matrices. This resulted in a median seasonal dispersal distance of 377 m (inter-quartile range 95 - 1114) for juveniles and 180 m (inter-quartile range 19 – 1062) for adults.

Supplementary table 4: AIC values of three different distributions fitted to between-season dispersal distance

	Weibull	Gamma	Exponential		
				Weibull parameters	
				Scale	Shape
Breeding season to post-breeding season					
Juvenile (n=40)	612	610	NA	668.2	0.64
Adult (n=77)	1123	1149	NA	459.4	0.39

Dispersal matrices

To link the dispersal kernels to the transmission simulation model, we estimated the probability to disperse to any location from the origin location, using an individual-based simulation analysis. We generated 1,000,000 random points within a grid cell, representing the origin location of birds. The grid size corresponded to the grid size used for the transmission simulation model. The distance that each bird moved was sampled from the dispersal kernel. The direction of the movement was generated from a uniform distribution. The destination grid cell was recorded for each bird. The proportion of birds that ended up in each grid cell was calculated to construct a movement matrix, see Supplementary figure 10 for a visualisation of the daily dispersal matrices. This matrix was applied to each location each day, where movements outside of the country borders were not allowed.

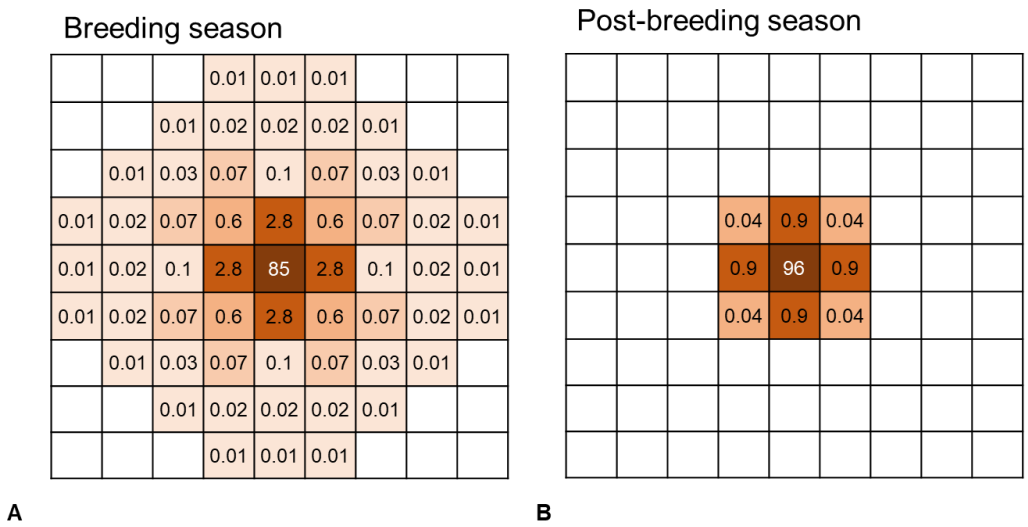

Supplementary figure 10: Visualisation of daily movement matrices for a) breeding season, b) post-breeding season. Values indicate the proportion of birds moving to that respective cell using the middle cell as origin location. Values lower than 0.01% are not shown.

Daily movement scenarios for extra reservoir host

To explore the movement behaviour of a potential additional reservoir host, we created two movement scenarios: increased movement and movement within uncertainty range (sensitivity analysis S3).

Increased movement scenario

As this reservoir population represents several species, the 'increased movement' scenario was created by mixing dispersal kernels of two bird species. We obtained estimates of movement distances for mallards from literature, because these have been found positive for USUV infection in the Netherlands and show movement behaviour distinct from blackbirds. Median movement distance for mallards outside the breeding season was estimated at 1.5 km [81]. Using roughly the same ratio between breeding and post-breeding movement as for blackbirds (daily movement in breeding season being around 3x further than in post-breeding season), we assumed daily movement in breeding season to be 4.5 km. We calculated the corresponding scale parameters (keeping the shape parameter constant) that resulted in a median movement distance of 4.5 km in breeding season and 1.5 km in post-breeding season (Supplementary table 5). These parameters were then combined with the blackbird movement parameters to create the 'increased movement' scenario: reservoir host movement behaviour consists of 80% blackbird and 20% mallard dispersal.

Movement within uncertainty range (sensitivity analysis)

We found blackbird movement distances in post-breeding season to be lower than in breeding season (Supplementary figure 8). To explore the implications of this finding we created a sensitivity analysis where movement in both seasons was parameterised as breeding season movement. This was used for both the blackbird and the reservoir population.

Resulting dispersal kernels are shown in Supplementary figure 11 and corresponding parameters are shown in Supplementary table 5.

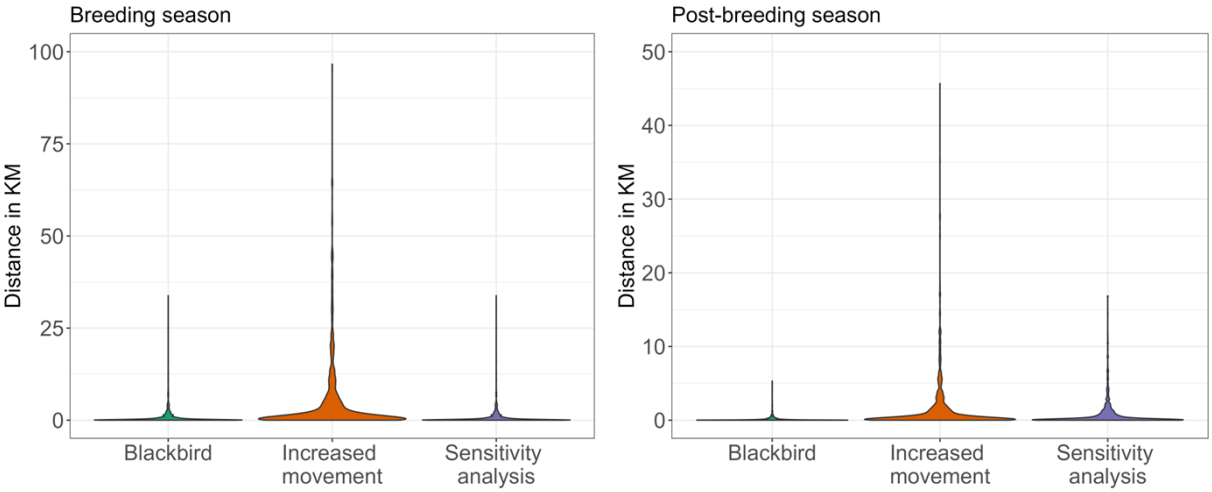

Supplementary figure 11: Daily movement kernels for blackbirds and the two scenarios.

Supplementary table 5: Daily movement parameters for blackbirds, mallards and the three mixture scenarios applied to the additional reservoir population.

	Weibull parameters		**Distance in meters**	
	Scale	**Shape**	**Median**	**Interquartile range**
Breeding season				
Blackbird	329.4	0.44	143	19 - 692
Mallard	10376	0.44	4,515	613 – 21,837
Increased movement scenario	2339	0.44	1,016	138 – 4,913
Movement sensitivity analysis	329.4	0.44	143	19 - 692
Post-breeding season				
Blackbird	63.4	0.46	29	4 - 129
Mallard	3329	0.46	1,500	222 – 6,776
Increased movement scenario	716	0.46	323	47 – 1,458
Movement sensitivity analysis	329.4	0.44	143	19 - 692

Supplementary Material C: Surveillance data

A more detailed description of the surveillance data can be found in Münger et al. [18].

PCR and serology testing in live birds (datasets 1 & 2)

Live free-ranging birds were sampled by trained volunteer ornithologists at different locations throughout the Netherlands between March 2016 and December 2022. Sampling was performed under ethical permits AVD801002015342 and AVD80100202114410 issued to NIOO-KNAW. Birds were captured using mist nets and ringed, after which a throat swab, a cloacal swab, and a blood sample were collected. Viral diagnostics was done by RT-PCR on throat and cloacal swabs. Bird sera were screened for USUV and WNV antibodies in a protein micro-array, where positive samples were subsequently tested for viral neutralization using Virus Neutralization Tests (VNT) and Focus Reduction Neutralization Tests (FRNT) as previously described [35,36].

Reporting and PCR testing of dead birds (datasets 3 & 4)

Dead free-ranging birds were reported through a citizen science-based alerting system run jointly by Sovon and the Dutch Wildlife Health Centre (DWHC) between March 2016 and December 2022 [84]. A selection of the reported dead birds, based on the freshness of the carcasses (death within ca. 24h) and the likelihood of disease being the cause of death was collected, necropsied, and samples were taken. From 2016 to 2018, dead blackbirds were tested for USUV by RT-PCR if necropsy indicated USUV as a possible cause of death; from 2019, all submitted birds were tested. In 2016, dead blackbirds submitted for post-mortem examination were selectively chosen by the DWHC to determine the expansion of the USUV outbreak in 2016. So, the analysed dead birds were mainly selected from areas where USUV had not been detected previously but within several kilometres from where it had been. From 2017 onwards, the selection of fresh dead birds for post-mortem examination was random over the Netherlands.

Blackbird population trends (dataset 5)

Population trends for the Dutch blackbird population were derived from a national breeding bird monitoring scheme [60]. This scheme consists of standardised counts in thousands of sample sites (plots) by voluntary observers. Each year, multiple visits (5-10) within the breeding season (March-July) were used to derive the number of territories. These territories were determined based on species-specific interpretation criteria, including behaviour observed, detection probabilities, and timing of observation.

Supplementary Material D: Inference approach

The ABC-SMC algorithm

The ABC-SMC algorithm used here enhances the basic ABC algorithm by incorporating two main steps: weighted resampling of simulated particles and a gradual reduction in tolerance. Our specific implementation of the algorithm improves upon [85] original algorithm in three ways: (1) an adaptive threshold schedule selection based on quantiles of distances between simulated and observed data [86, 87] (2) an adaptive perturbation kernel width during the sampling step, dependent on the previous intermediate posterior distribution [54,83], and (3) the capability to use multiple criteria simultaneously. The algorithm proceeds as follows:

Step 1: Definition of summary statistics, distances, and model

- **Summary statistics:** Define the summary statistics *S* that adequately capture the essential features of the observed data. We used five summary statistics (Supplementary figure 13): (i) seroprevalence in live blackbirds for each month and region (North, Middle, South), (ii) PCR prevalence in live blackbirds for each month and region, (iii) PCR prevalence in dead blackbirds for each month and region, (iv) annual relative blackbird population size for each region and (v) the relative number of reported dead blackbirds per year within each region. Regions were created by dividing the country into three equally sized regions (Supplementary figure 12).

- **Distances:** Define distance functions $D_1, D_2, \ldots, D_5$. For the three first summary statistics the negative log-likelihood was used as distance measure:

$$D_{1-3} = -\sum_{y=2016}^{y=2022} \sum_{m=4}^{m=10} \sum_{c=1}^{c=3} \log\left(Binomial(y, n, p)\right)$$

where y is the number of positive samples in the data, n is the total number of samples in the data, and p is the (sero)prevalence in the model simulation for seroprevalence in live blackbirds (D1), PCR prevalence in live blackbirds (D2), and PCR prevalence in dead blackbirds (D3). Likelihood values were summed across years (y, 2016 to 2022), months (m, April to October), and regions (c, North, Middle, and South).

For the last two summary statistics, distance was calculated as the sum of squared differences between observed and simulated datapoints for each year (y, 2016 to 2022) and region (c, North, Middle, and South):

$$D_{4-5} = \sum_{y=2016}^{y=2022} \sum_{c=1}^{c=3} \left(M_{y,c} - D_{y,c}\right)^2$$

where $D_{y,c}$ and $M_{y,c}$ are the relative number of dead blackbirds (D4) or the relative blackbird population size (D5) per year and region in the data and model respectively.

- **Model definition:** Define the model $M(\theta)$ which takes a parameter vector θ and generates simulated data from which summary statistics are calculated. Each model replicate was simulated 3 times using the same parameter set to reduce the impact of stochasticity. Distances were calculated for each simulation, but the acceptance decision was based on the average of these three distances.

Step 2: Particle generation

- **First iteration** (t = 1):

- Generate N particles θ_i by drawing $\theta_i \sim \pi(\theta)$, where $\pi(\theta)$ is the prior distribution.

- **Subsequent iterations** ($t > 1$):

  - Draw θ_i from the set of particles accepted at iteration $t - 1$ with probability proportional to their weights $w^{(t-1)}$.

  - **Particle perturbation:** New particles were generated by perturbing each parameter $\theta_{i,k}$ (where k indexes the parameters of θ) using a Gaussian kernel with a standard deviation $\sigma_k^{(t-1)}$ of 0.5 times the empirical standard deviation of the accepted particles for that parameter in the previous iteration:

$$\theta_{i,k} = \theta'_{i,k} + \eta_k, \quad \eta_k \sim \mathcal{N}(0, \sigma_k^{(t-1)})$$

    where $\sigma_k^{(t-1)}$ is the standard deviation of parameter k in the accepted particles at iteration $t - 1$.

  - **Check perturbed particle:** If any perturbed parameter $\theta_{i,k}$ is outside the prior distribution $\pi(\theta_{i,k})$, reject the perturbed particle and repeat the particle generation step until $\theta_{i,k}$ lies within $\pi(\theta)$.

Step 3: Running the model and calculating summary statistics and distances

For each particle θ_i:

- Run the model $M(\theta_i)$ to obtain simulated data.
- Calculate summary statistics $S_{\text{model}}(\theta_i)$ for the simulated data.
- Compute the distances $D_1, D_2, \ldots, D_5$ between the summary statistics $S_{\text{model}}(\theta_i)$ and the summary statistics S_{obs} of the observed data:

$$D_j(\theta_i) = \text{distance}(S_{\text{model},j}(\theta_i), S_{\text{obs},j}), \qquad j = 1,2,\ldots,5.$$

Step 4: Particle acceptance

- **First iteration** ($t = 1$): Accept all N particles as the initial sample from the prior distribution.

- **Subsequent iterations** ($t > 1$): Accept particle θ_i if and only if $D_j(\theta_i) < \epsilon_j^{(t)}$ for all distances $j = 1,2,\ldots,5$. This means that a particle was only accepted when the distances of all summary statistics were below their respective threshold values.

Step 5: Calculation of associated weight

- **First iteration** ($t = 1$): Set weight for each accepted particle θ_i as $w_i = 1$.

- **Subsequent Iterations** ($t > 1$): Compute the weight for each accepted particle θ_i as:

$$w_i = \frac{\pi(\theta_i)}{\sum_{j=1}^{N} w_j^{(t-1)} K(\theta_i | \theta_j, \Sigma^{(t-1)})}$$

  where $K(\theta_i|\theta_j, \Sigma^{(t-1)})$ is the perturbation kernel centered at θ_j

Step 6: Repeat steps 2 to 5 until N particles are accepted

Step 7: Normalise the weights

$$w_i^{(t)} = \frac{w_i}{\sum_{j=1}^{N} w_j}$$

Step 8: Calculation of new thresholds from the 75th percentile values of $D_1, D_2, \ldots, D_5$

$$\epsilon_j^{(t+1)} = \text{Percentile}(D_j(\theta_1), D_j(\theta_2), \ldots, D_j(\theta_N), 75\%)$$

Step 9: Increment the iteration number

- Set $t = t + 1$.
- Go back to step 2 and repeat the process until convergence criteria are met.

The algorithm was run until the acceptance rate (number of particles accepted over the total number of particles tested during an iteration) reached 5% or lower. Convergence of the posterior distributions was confirmed by visual inspection of intermediate distributions of consecutive generations and by visual inspection of the threshold value of consecutive generations. Minor reductions in threshold values across generations suggests the algorithm has converged.

The algorithm was run using 3 independent chains, where each chain generated 200 accepted parameter sets for each generation. The last posterior distribution therefore consisted of 600 accepted particles.

Design of summary statistics

The observation process, when known, was accounted for in three ways. When no data were available for a specific month-region combination, the distance for that data point was not calculated. Secondly, in the model, prevalence in dead birds was calculated among birds that died the previous day to reflect the data collection process where only recently-died birds were submitted for testing. Thirdly, model-predicted population size was calculated by averaging the period April to July, similar to when counts were conducted to estimate population size [60]. Distances between the observed and simulated summary statistics were calculated for each summary statistic separately, with each summary statistic having its own threshold value for acceptance. For the three (sero)prevalence-based summary statistics the likelihood of the observed prevalence was used as distance measure. For the summary statistics related to population size and dead blackbird count, the distance was calculated as the sum of squared differences between observed and simulated datapoints.

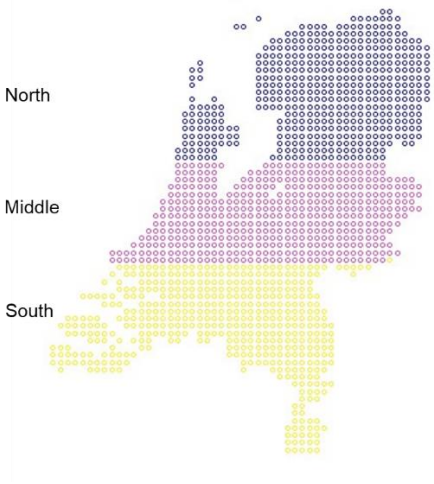

Supplementary figure 12: Division of the Netherlands into three equally sized regions.

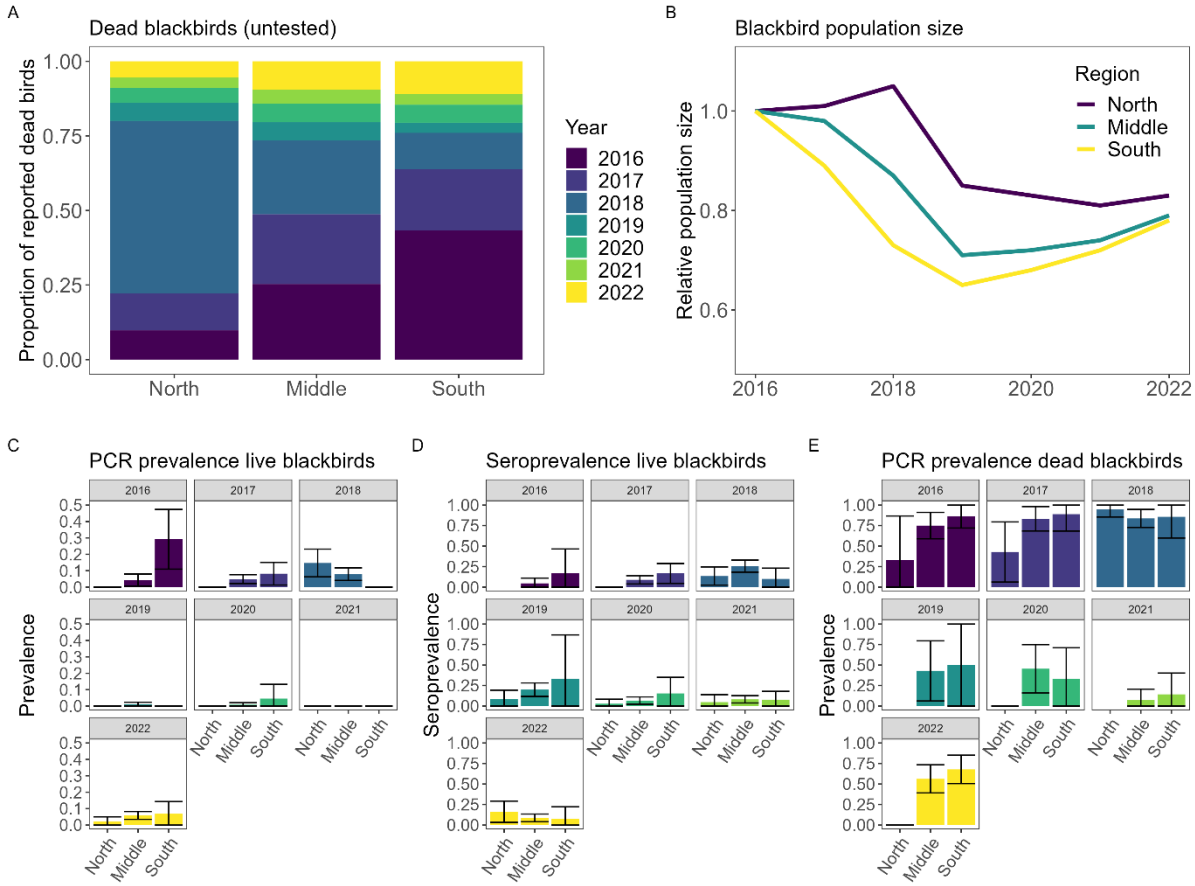

Supplementary figure 13: Overview of surveillance data by year and region. One summary statistic was constructed for each of the datasets.

Prior distributions

All prior distributions were uniformly distributed. We discuss each parameter's definition, chosen prior and reasoning behind our choices.

Re-emergence rate

Definition: Fraction of the prevalence in mosquitoes in September that persists to the subsequent spring

Prior: 0 to 0.3

Justification: It is largely unknown which overwintering processes play a role in USUV re-emergence. One possible route is through vertical transmission in diapausing mosquitoes. Estimates of the efficiency of this route are lacking for USUV in *Cx. pipiens* mosquitoes. For other viruses and mosquitoes estimates are available such as for dengue where studies found vertical infection rates were often very low, but could get up to 13% [89]. Due to a lack of estimates for *Cx pipiens* and USUV and to allow for alternative routes such as maintenance in birds or reintroductions, we assumed a maximum re-emergence rate of 0.3.

Transmission probability bird to mosquito

Definition: Probability that a mosquito gets infected upon a bite on an infectious bird

Prior: 0 to 1

Justification: Variation in values used in other models and in experimental studies is large, e.g. a value of 12.5% was used in Rubel et al.'s USUV model [64], while Turell et al. found 81% of mosquitoes infected after oral exposure to WNV [90]. We therefore did not restrict the range of possible values and allowed for values between 0 and 1.

Abundance scaling parameter

Definition: Multiplication factor for host population size. This converts the host and vector abundance to be on the same scale, such that their ratio reflects the vector-to-host ratio

Prior: 0.03 to 2

Justification: This includes a wide range of vector-to-host ratios, ranging from around 1043:1 to 7:1 measured on August 15th (the period where mosquito size peaks). Exact estimates vary depending on other parameters as the extent of transmission and the disease-induced mortality rate affect the bird population size. The lower bound of 0.03 ensures that the mean starting abundance is at least 26 blackbirds per grid cell, as otherwise the population size becomes unreasonably and impractically small.

Disease-induced mortality rate in birds

Definition: Rate at which infectious birds die from infection

Prior: 0.1 to 1

Justification: Significant mortality has been observed and reported following USUV infection, with first estimates of about 30% of infected blackbirds dying [64]. We therefore set the prior distribution between 1 and 10 days until death.

Historical annual force of infection (FOI)

Definition: Rate at which susceptible hosts became infected per year prior to 2016. This determines the level of immunity present in birds at the start of 2016.

Prior: 0 to 0.3

Justification: There is no evidence of PCR-positive birds before 2016 in the Netherlands. The lower bound of the prior distribution is therefore set to 0. The seroprevalence in autumn 2016 was estimated at 4.7% (95%CI 0-11%) in the middle region and at 17% (95%CI 0-46%) in the southern region. The estimates were all based on samples are from September and October, so after transmission was detected. No significant changes in the blackbird population size were observed prior to 2016. We therefore assume that the maximum amount of transmission prior to 2016 was the seroprevalence in 2016 + 1*SE and use this as the upper bound of the historical FOI. This corresponds to a historical FOI of 0.30.

Relative biting rate on additional reservoir host compared to blackbirds

Definition: The relative frequency at which the additional reservoir host receives bites compared

	to blackbirds. This is a consequence of both biting preference and differences in bird density.
Prior	0 to 50
Justification	A large prior distribution was chosen here, because it is difficult to estimate as the distribution of mosquito bites is a consequence of biting preference and relative host abundance. The reservoir host represents several possible (unknown) host species, making it difficult to estimate its relative abundance and attractiveness to mosquitoes. We therefore chose a wide prior and ensured that the posterior distribution was fully informed by the data and not restricted by the prior distribution.

<u>Reservoir population's lifespan</u>

Definition	Mean lifespan of the additional reservoir population. The inverse of this value represents the daily mortality rate.
Prior	365 to 7305 days (1 to 20 years)
Justification	As we wanted to characterise this population from the epidemiological data, we selected a wide prior that contains the vast majority of plausible values.

Supplementary Material E: Validation of inference approach

We created five different simulated datasets, using values shown in Supplementary table 6. These datasets were created from the blackbird-only model (model A) using a regional-level parameter for the historical FOI. A total of seven parameters were estimated: 1) re-emergence rate, the fraction of the USUV prevalence in mosquitoes in September that persists to the subsequent spring, 2) transmission probability bird-to-mosquito, 3) abundance scaling parameter, this converts the host and vector abundance to be on the same scale, meaning that their ratio reflects the vector-to-host ratio, 4) disease-induced mortality rate in blackbirds, 5-7) historical FOI by region (North, Middle, South), to quantify transmission prior to first detection leading to non-zero immunity levels in 2016.

The ABC-SMC algorithm, hyperparameters, and summary statistics were identical to those used for fitting to the real surveillance data, see Supplementary Material C.

Supplementary table 6: Parameter values used to create simulated datasets for inference validation.

Set	Re-emergence rate	Transmission probability bird to mosquito	Abundance scaling parameter	Disease-induced mortality rate	Historical FOI		
					North	Middle	South
A	0.25	0.7	0.2	0.2	0.10	0.25	0.20
B	0.25	0.8	0.15	0.3	0.08	0.08	0.08
C	0.2	0.9	0.4	0.2	0.20	0.20	0.05
D	0.2	0.5	0.15	0.1	0.04	0.04	0.04
E	0.1	0.6	0.1	0.4	0.01	0.01	0.10

Inference validation results

The re-emergence rate, abundance scaling parameter, transmission probability, and disease-induced mortality rate were well estimated with 19/20 (95%) true values falling within the estimated 95% highest density intervals (HDI) of the posterior distributions across the five datasets (Supplementary figure 14). We calculated concordance coefficients to quantify the agreement between parameter's true values and the estimated median values from the posterior (Supplementary figure 15). We found that the abundance scaling parameter and disease-induced mortality rate were best approximated by the posterior median. The inference framework was unable to estimate the values of the historical FOI in all three regions within the range of the chosen prior. Due to the limited identifiability of this parameter, we did not use regional-level parameters when fitting the model to the real surveillance data, but instead assumed the same value throughout the country.

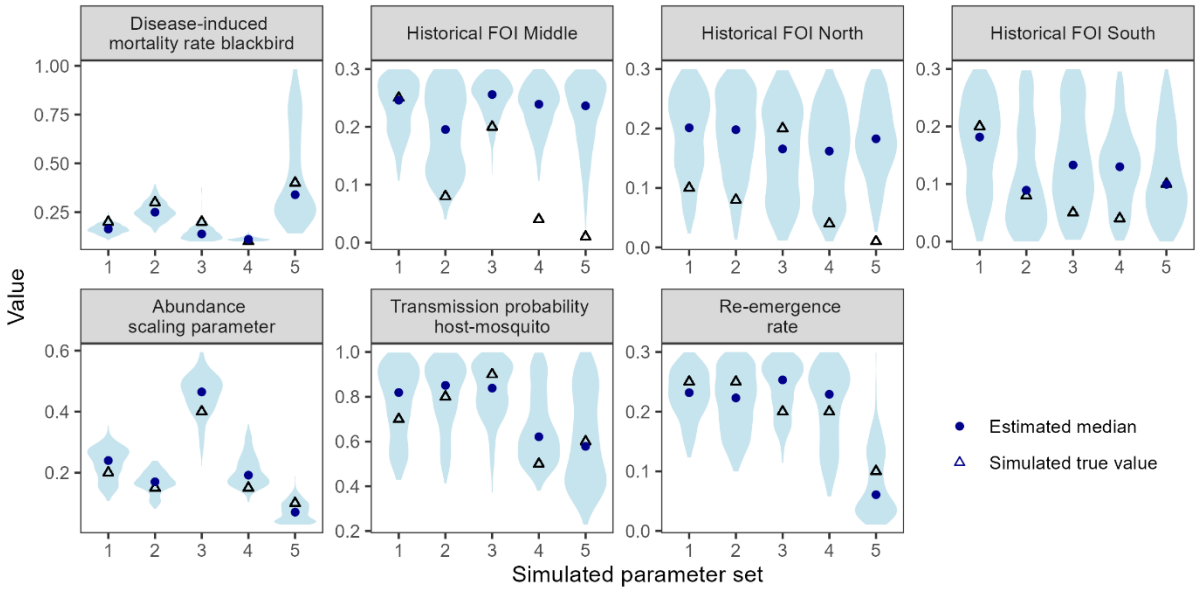

Supplementary figure 14: Estimated parameters from five simulated datasets (1-5) with the true value used in the simulation (blue triangle), the estimated median (blue circles) and posterior distributions (blue violins). Each estimate was based on two independent chains with 200 accepted particles each.

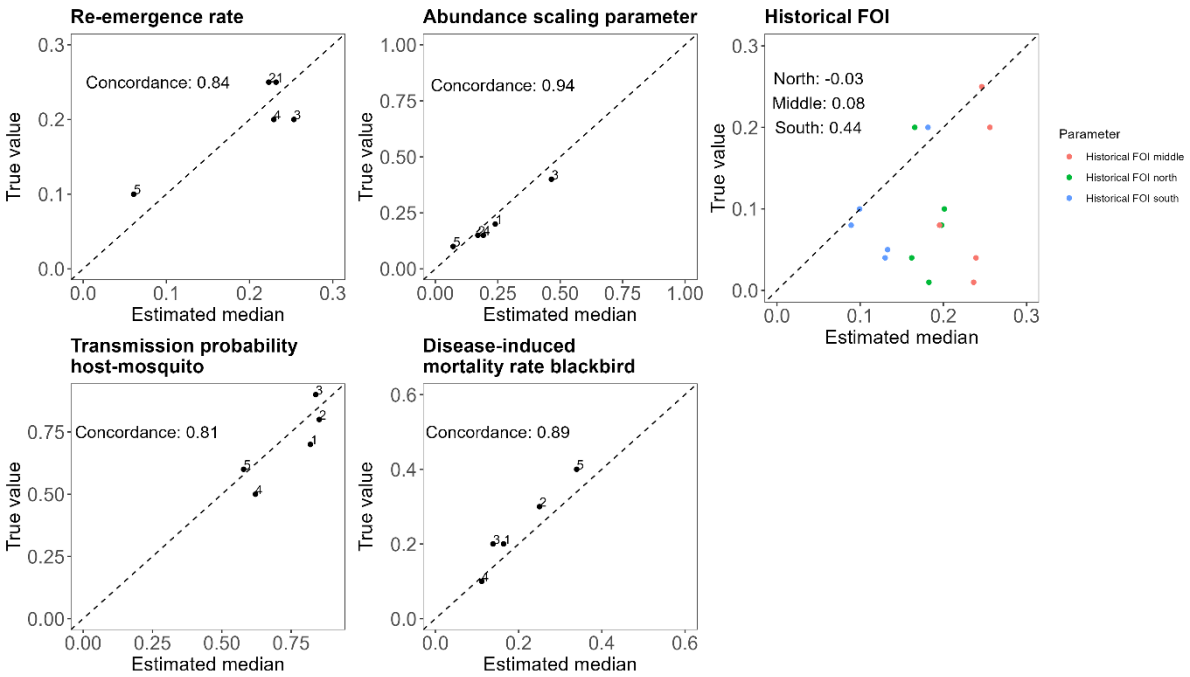

Supplementary figure 15: Concordance between parameter's true values and the estimated posterior median values across five simulated datasets (1-5). Concordance represents the strength of the relationship y=x. A value of 1 indicates perfect agreement, while 0 indicates poor agreement.

Supplementary Material F: Additional results

Fits of main model (model D)

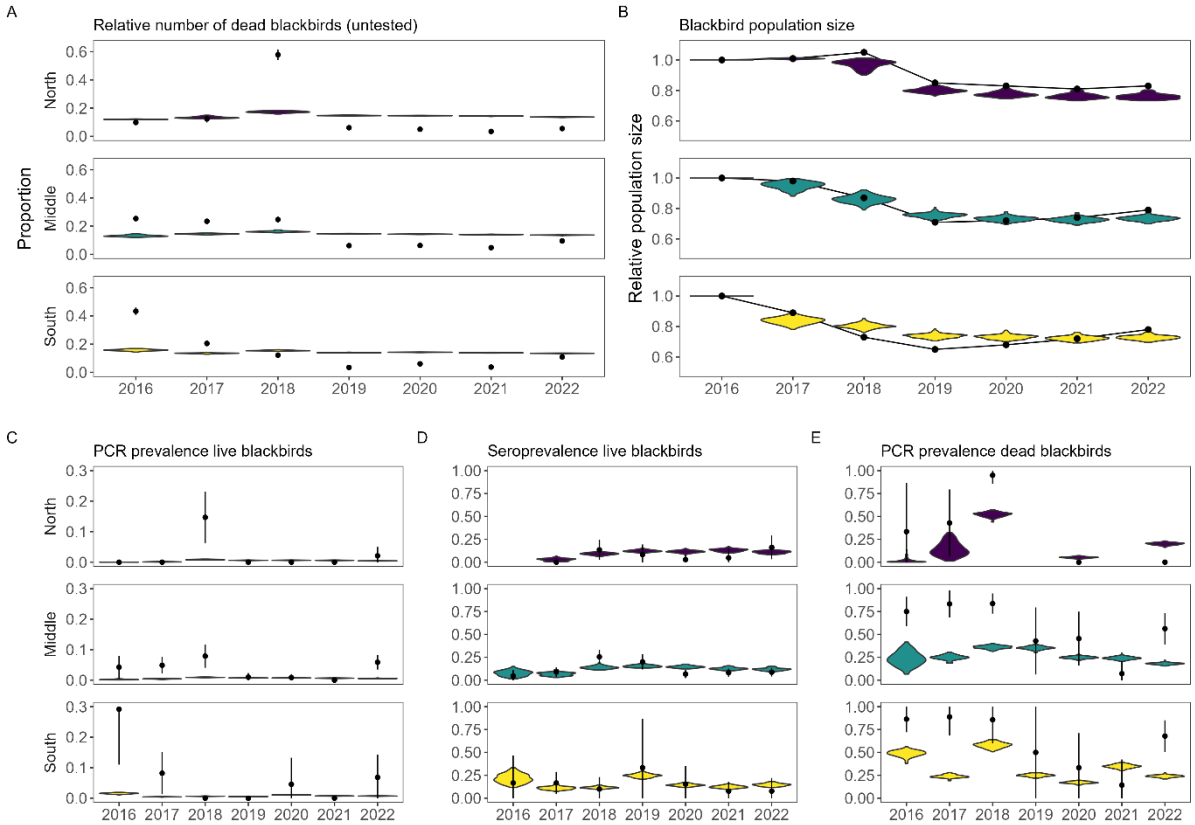

Supplementary figure 16: Resulting model fits from best-fitting model obtained by comparing model predictions (violins) to observed data (in black, with dots representing the mean and vertical lines representing binomial 95% confidence intervals). Model predictions are based on 100 simulations using random draws from parameter sets from posterior distributions. Results are aggregated across time to annual level. Results on within-year level are available in Supplementary figure 18. For figures C-E, predictions are only calculated for those months and regions when surveillance data was available. The period for which model predictions were calculated therefore varies between years and regions to ensure alignment with the observation process.

Seroprevalence

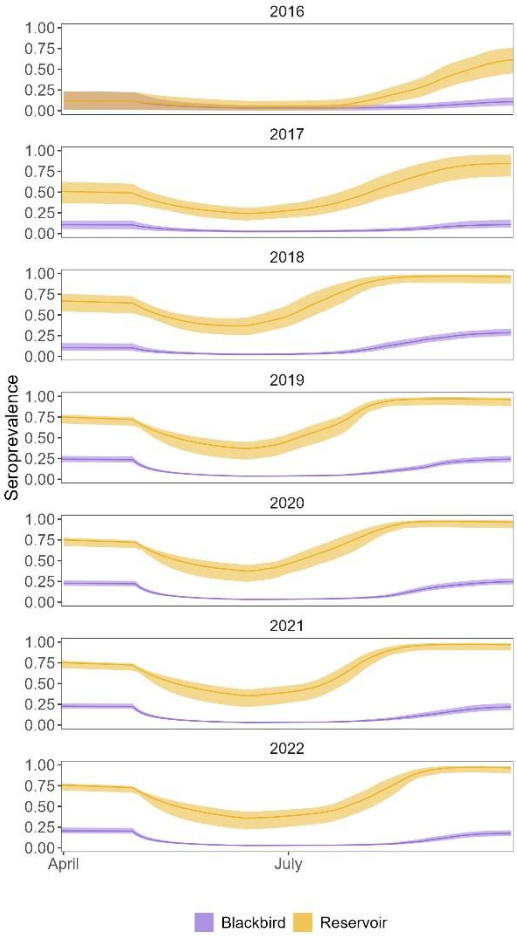

Supplementary figure 17: Predicted seroprevalence in blackbird and reservoir population. Model predictions are based on 100 simulations using random draws from parameter sets from posterior distributions.

Model fits over time for model D

In addition to the regional disaggregation of model fits presented in Supplementary figure 16, the prevalence-based patterns could also be disaggregated to monthly estimates. Fits to within-year trends in the data are shown for these three summary statistics (Supplementary figure 18).

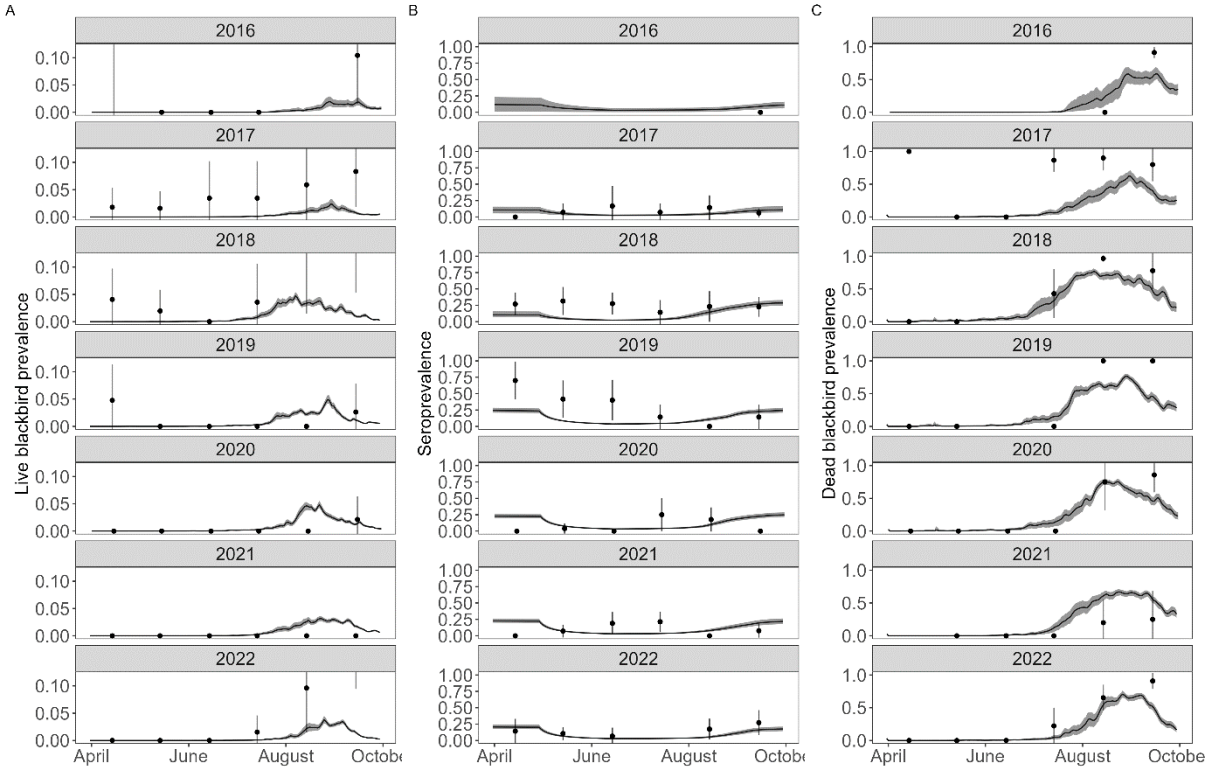

Supplementary figure 18: Comparison of observed (dots with vertical lines representing 95% confidence intervals) and simulated data from best-fitting model at monthly level for A) live blackbird infection prevalence, B) live blackbird seroprevalence, and C) dead blackbird infection prevalence. Model predictions are based on 100 simulations using random draws from parameter sets from posterior distributions. Observed data are aggregated to monthly level.

Model comparison for sensitivity analyses

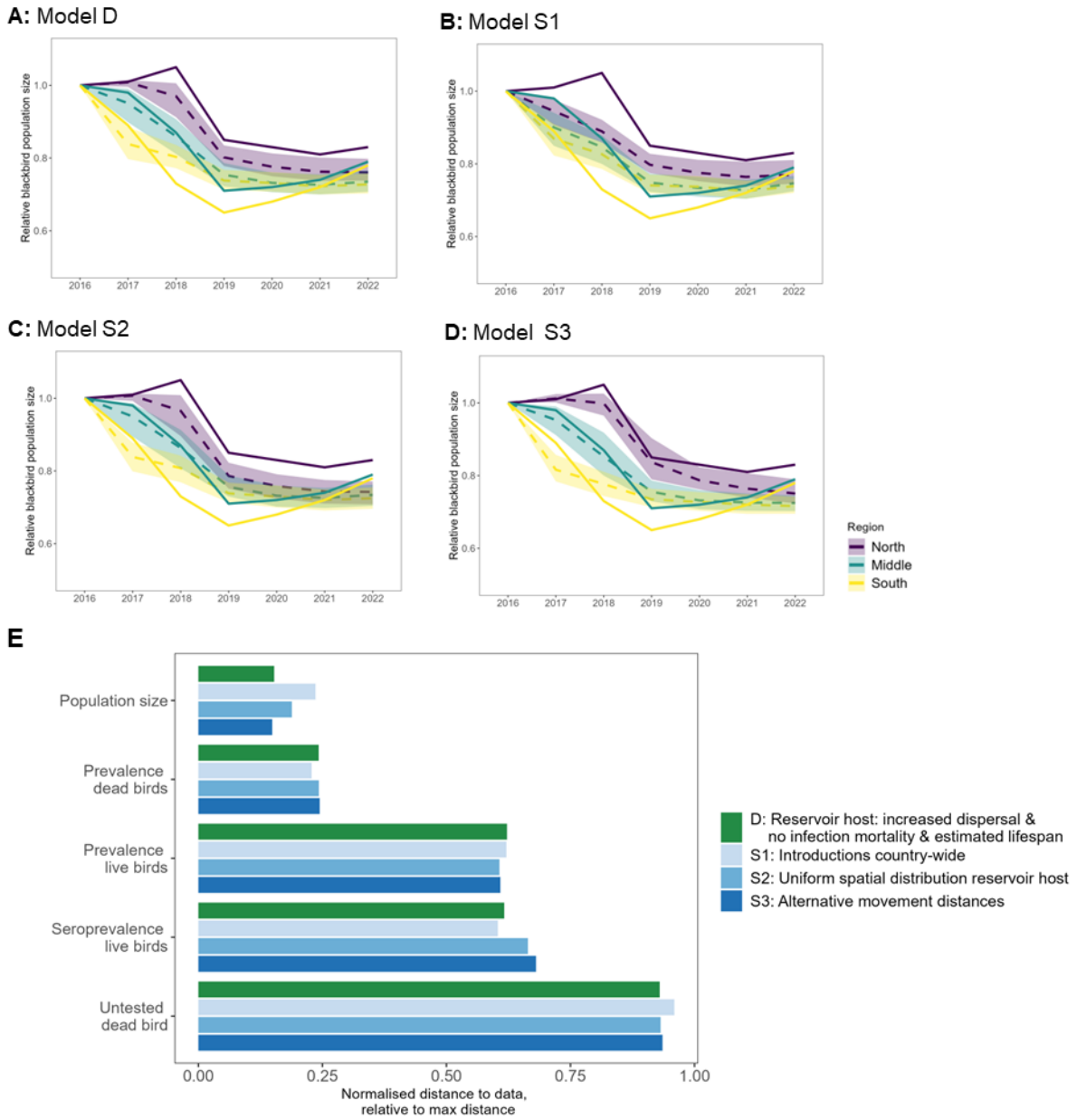

Supplementary figure 19: Comparison of model versions for sensitivity analyses. A-D) Visual fit of simulated data (dashed lines with 95% prediction interval) to observed data (solid lines) for the blackbird population size. Results are shown for the best-fitting model (main model D), and the three sensitivity analysis models S1-S3. E) Comparison of model fits between best-fitting model and sensitivity analysis models. Comparisons were based on distances between observed and simulated data for each data set. For each data set, distances were normalised by dividing each model's distance by the maximum across all model versions. A normalised distance of 1 thus indicates that this model showed the largest distance between observed and simulated data (i.e. worst fit). Lower normalised distances indicate a better fit to the data.

Model fits of alternative models

Below we show the model fits for all alternative models (models A-C and S1-S3), similar to supplementary Supplementary figure 16.

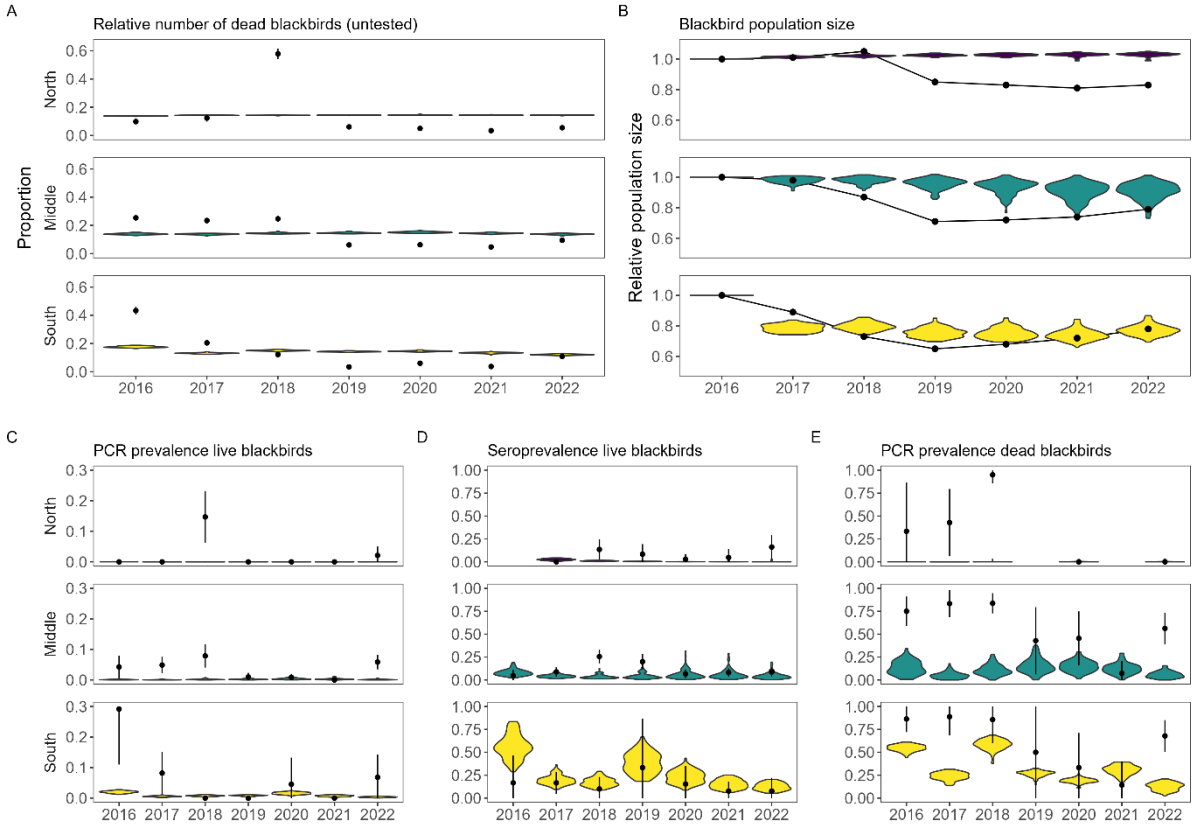

Supplementary Figure 20: Resulting model fits from model A obtained by comparing model predictions (violins) to observed data (in black, with dots representing the mean and vertical lines representing binomial 95% confidence intervals). Model predictions are based on 100 simulations using random draws from parameter sets from posterior distributions. Results are aggregated across time to annual level. For figures C-E, predictions are only calculated for those months and regions when surveillance data was available. The period for which model predictions were calculated therefore varies between years and regions to ensure alignment with the observation process.

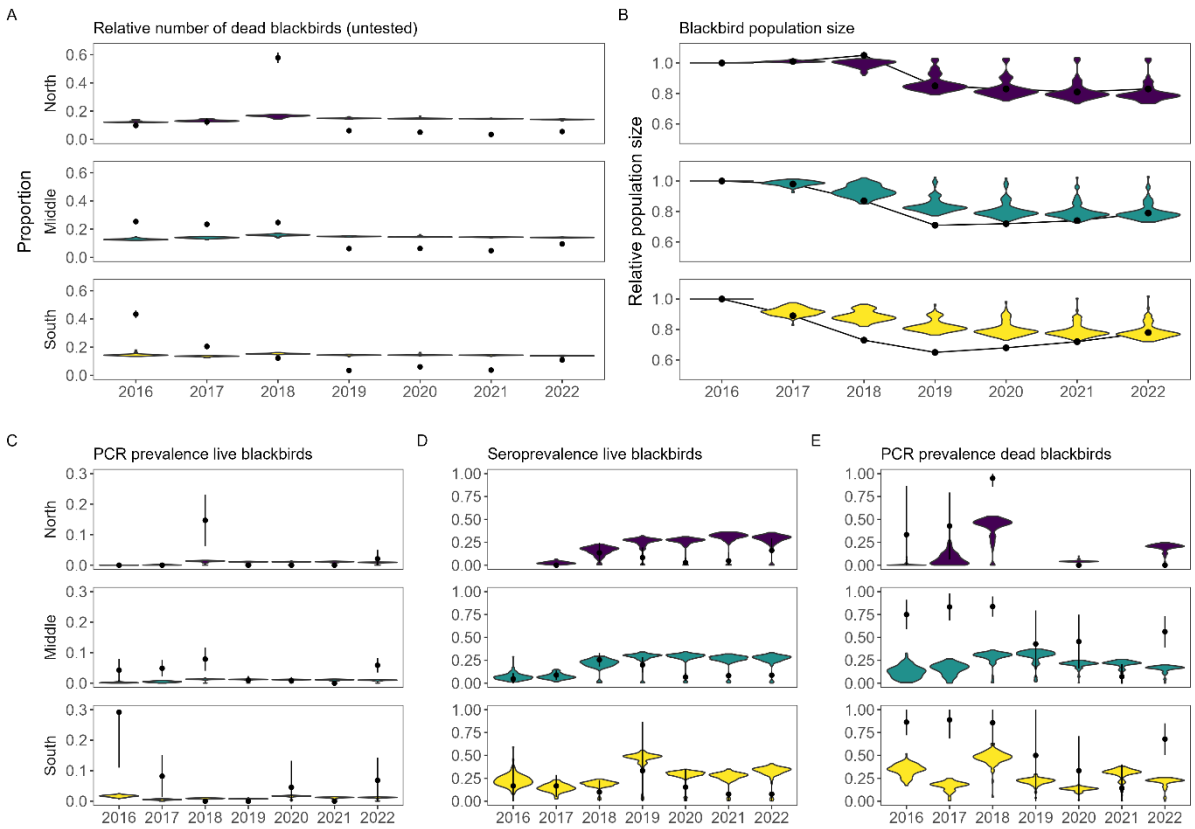

Supplementary figure 21: Resulting model fits from model B obtained by comparing model predictions (violins) to observed data (in black, with dots representing the mean and vertical lines representing binomial 95% confidence intervals). Model predictions are based on 100 simulations using random draws from parameter sets from posterior distributions. Results are aggregated across time to annual level. For figures C-E, predictions are only calculated for those months and regions when surveillance data was available. The period for which model predictions were calculated therefore varies between years and regions to ensure alignment with the observation process.

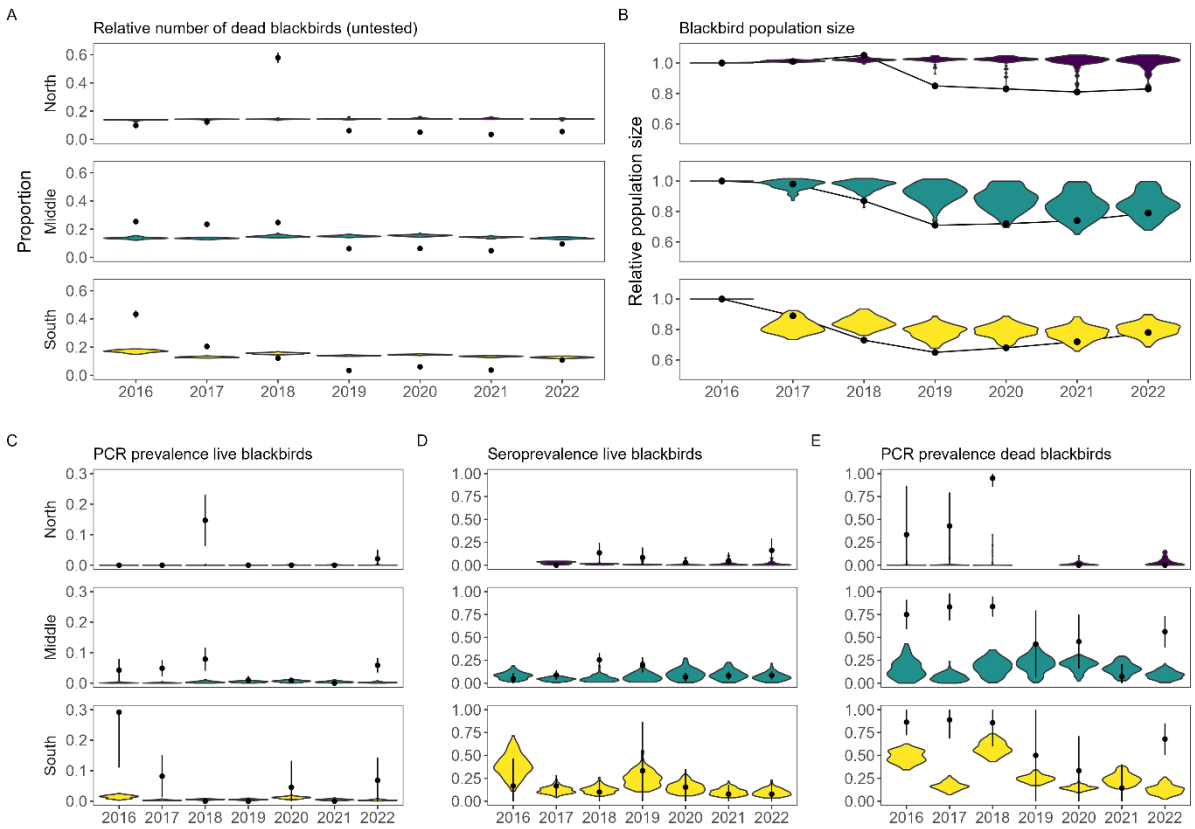

Supplementary figure 22: Resulting model fits from model C obtained by comparing model predictions (violins) to observed data (in black, with dots representing the mean and vertical lines representing binomial 95% confidence intervals). Model predictions are based on 100 simulations using random draws from parameter sets from posterior distributions. Results are aggregated across time to annual level. For figures C-E, predictions are only calculated for those months and regions when surveillance data was available. The period for which model predictions were calculated therefore varies between years and regions to ensure alignment with the observation process.

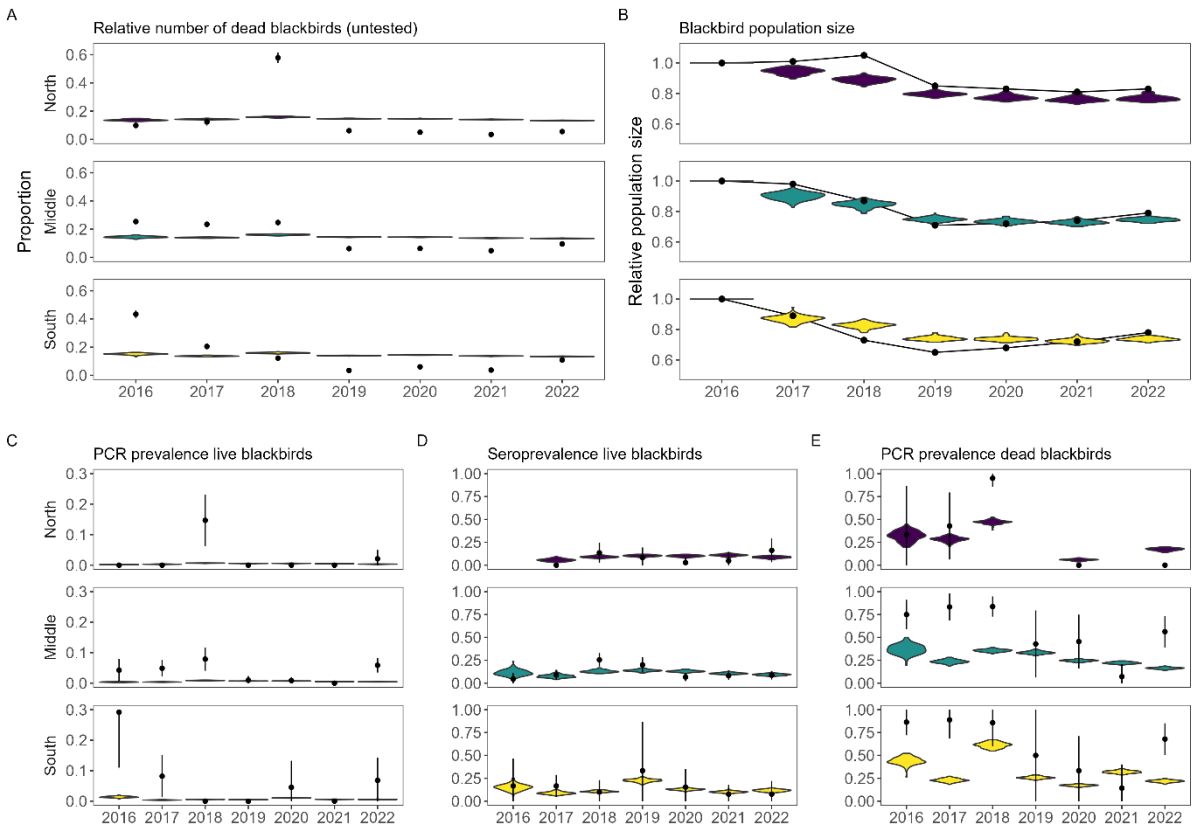

Supplementary figure 23: Resulting model fits from model S1 obtained by comparing model predictions (violins) to observed data (in black, with dots representing the mean and vertical lines representing binomial 95% confidence intervals). Model predictions are based on 100 simulations using random draws from parameter sets from posterior distributions. Results are aggregated across time to annual level. For figures C-E, predictions are only calculated for those months and regions when surveillance data was available. The period for which model predictions were calculated therefore varies between years and regions to ensure alignment with the observation process.

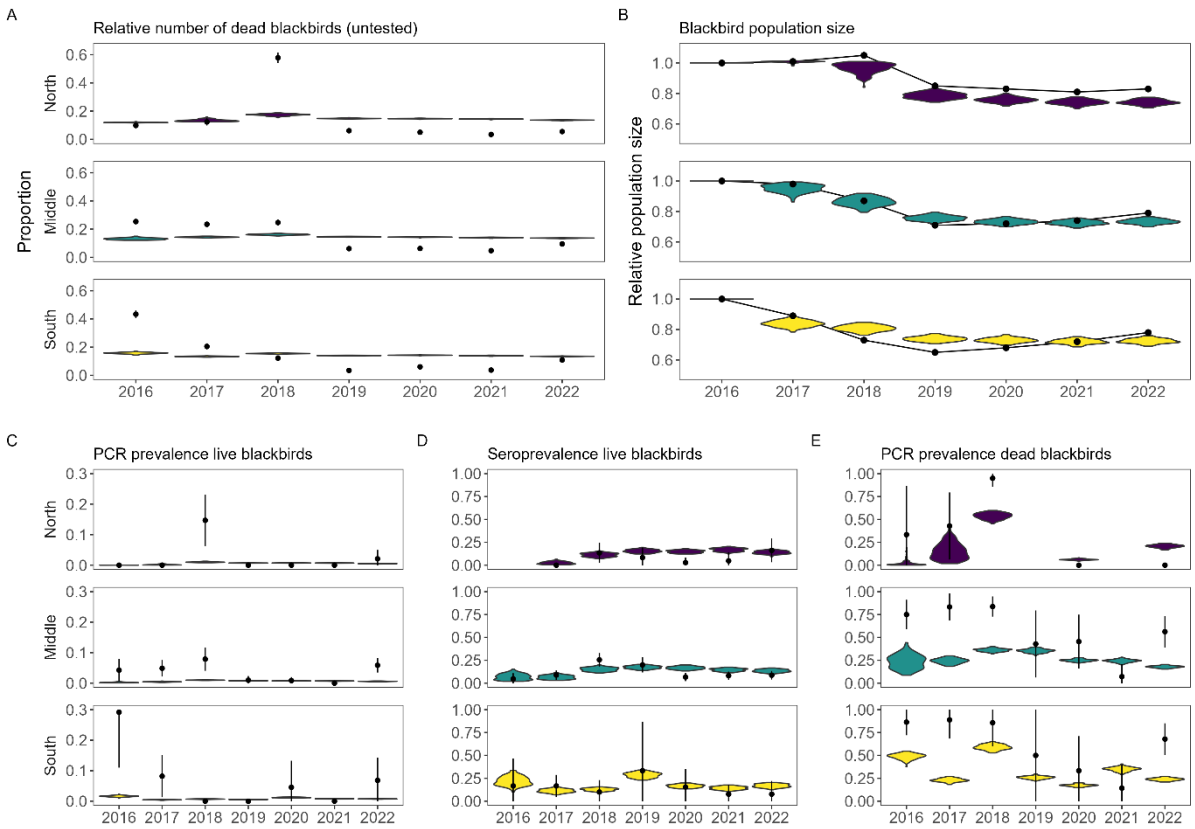

Supplementary figure 24: Resulting model fits from model S2 obtained by comparing model predictions (violins) to observed data (in black, with dots representing the mean and vertical lines representing binomial 95% confidence intervals). Model predictions are based on 100 simulations using random draws from parameter sets from posterior distributions. Results are aggregated across time to annual level. For figures C-E, predictions are only calculated for those months and regions when surveillance data was available. The period for which model predictions were calculated therefore varies between years and regions to ensure alignment with the observation process.

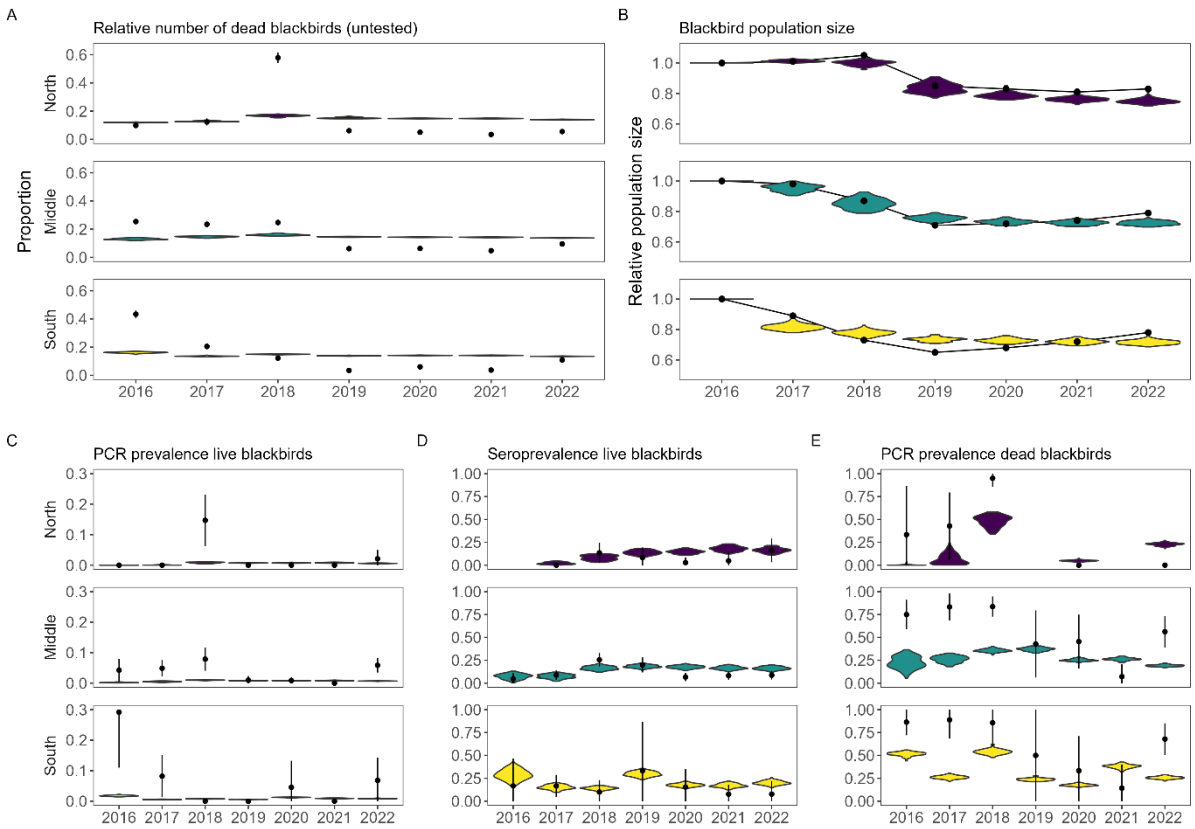

Supplementary figure 25: Resulting model fits from model S3 obtained by comparing model predictions (violins) to observed data (in black, with dots representing the mean and vertical lines representing binomial 95% confidence intervals). Model predictions are based on 100 simulations using random draws from parameter sets from posterior distributions. Results are aggregated across time to annual level. For figures C-E, predictions are only calculated for those months and regions when surveillance data was available. The period for which model predictions were calculated therefore varies between years and regions to ensure alignment with the observation process.

Posterior distributions of all models

Supplementary Table 7: Posterior estimates for each model version. Values shown are median estimates with 95% highest density intervals.

Model	Posterior parameter estimates (median and 95% highest density interval)						
	Re-emergence rate	**Transmission probability host-mosquito (p_{mb})**	**Abundance scaling parameter**	**Disease-induced mortality rate blackbirds (v)**	**Historical FOI**	**Lifespan reservoir (years) (1/ μ_{AR})**	**Relative biting frequency parameter (ω)**
A	0.01 (0.003-0.02)	0.91 (0.75-1.0)	0.04 (0.03-0.04)	0.52 (0.25-0.84)	0.17 (0.06-0.29)	NA	NA
B	0.19 (0.01-0.29)	0.68 (0.22-1.0)	0.08 (0.03-0.12)	0.25 (0.10-0.46)	0.09 ($2.6*10^{-4}$ – 0.27)	NA	45.6 (34.0-50.0)
C	0.004 ($9.1*10^{-4}$ - 0.01)	0.80 (0.51-1.0)	0.04 (0.03-0.07)	0.62 (0.26-0.98)	0.16 (0.02-0.28)	4.0 (1.0-7.1)	27.4 (8.2 – 49.4)
D	0.20 (0.08-0.30)	0.82 (0.45-1.0)	0.11 (0.06-0.15)	0.79 (0.60-1.0)	0.10 ($1.8*10^{-4}$ – 0.25)	6.8 (1.8-12.2)	34.8 (27.0-45.2)
S1	0.21 (0.11-0.30)	0.81 (0.44-1.0)	0.15 (0.08-0.21)	0.85 (0.67-0.99)	0.11 ($2.7*10^{-3}$ – 0.26)	8.0 (1.4-14.9)	28.0 (19.0-36.1)
S2	0.18 (0.07-0.30)	0.77 (0.41-0.99)	0.17 (0.09-0.27)	0.67 (0.50-0.86)	0.08 ($6.9*10^{-5}$ – 0.26)	7.6 (1.2-18.7)	38.3 (26.4-49.4)
S3	0.19 (0.05-0.28)	0.77 (0.49-0.99)	0.06 (0.03-0.09)	0.63 (0.50-0.82)	0.08 ($8.5*10^{-5}$ – 0.24)	2.8 (1.0-8.1)	44.0 (37.0-50.0)

Supplementary Material G: Inference diagnostics

A range of ABC diagnostics are shown in figures below. These are all based on the best-fitting model, model D.

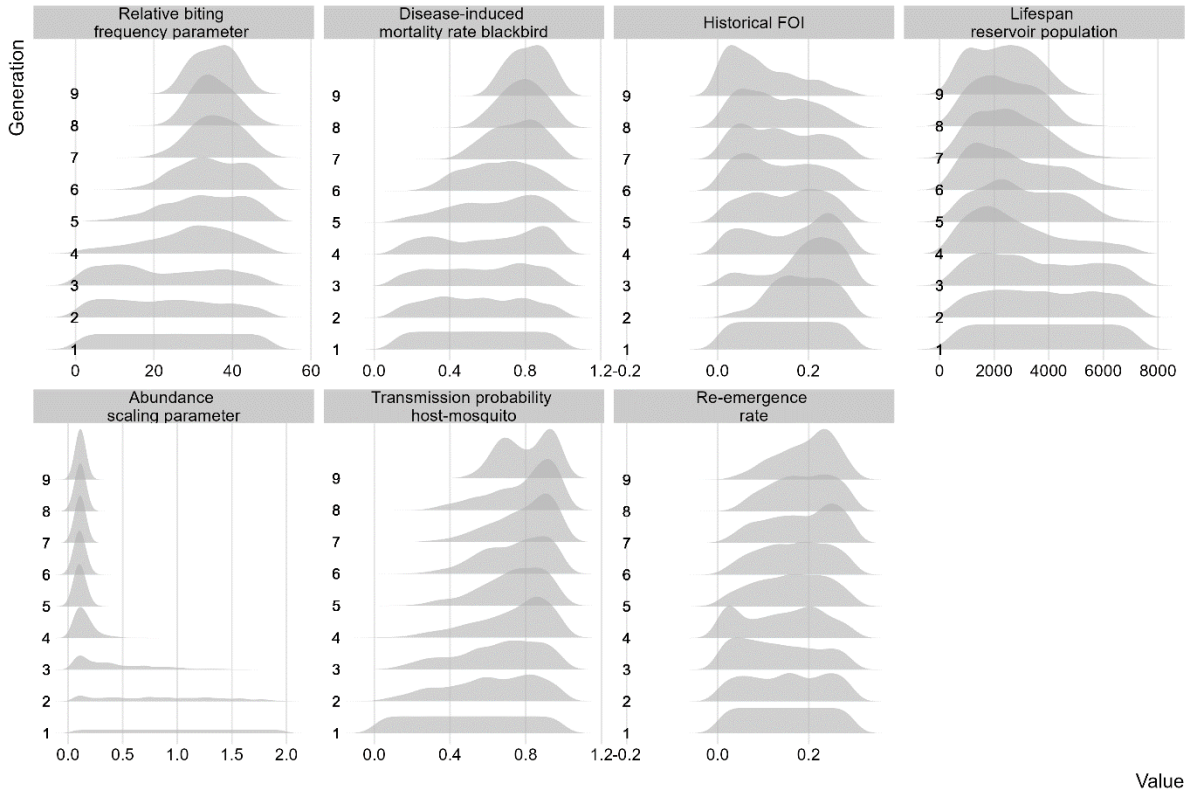

Supplementary Figure 26: Convergence of intermediate distributions towards the posterior distribution per generation for model D.

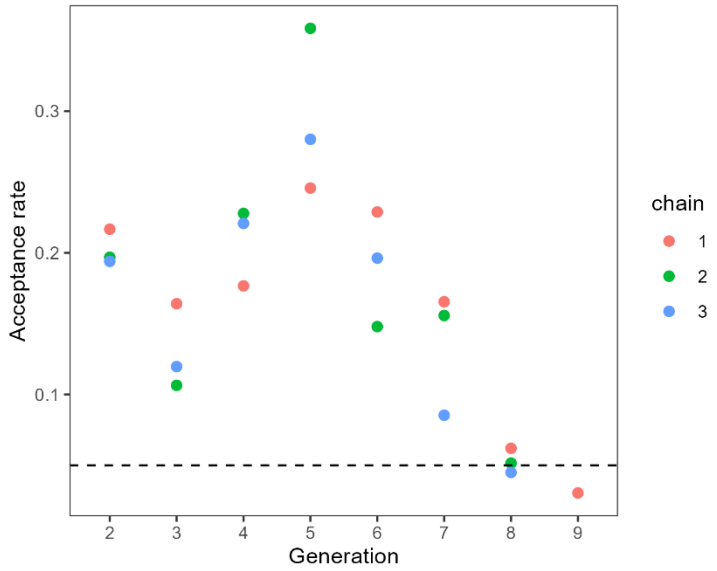

Supplementary figure 27: Acceptance rate of each chain per generation for model D. The horizontal dashed line represents the stopping criterion of a 5% acceptance rate.

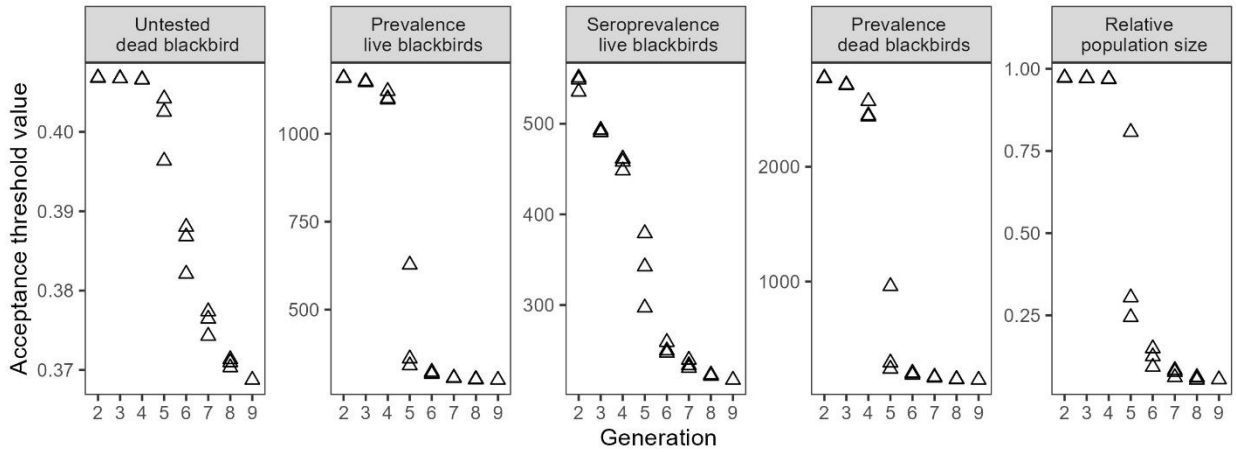

Supplementary figure 28: Development of increasingly strict threshold across generations for each of the summary statistics.

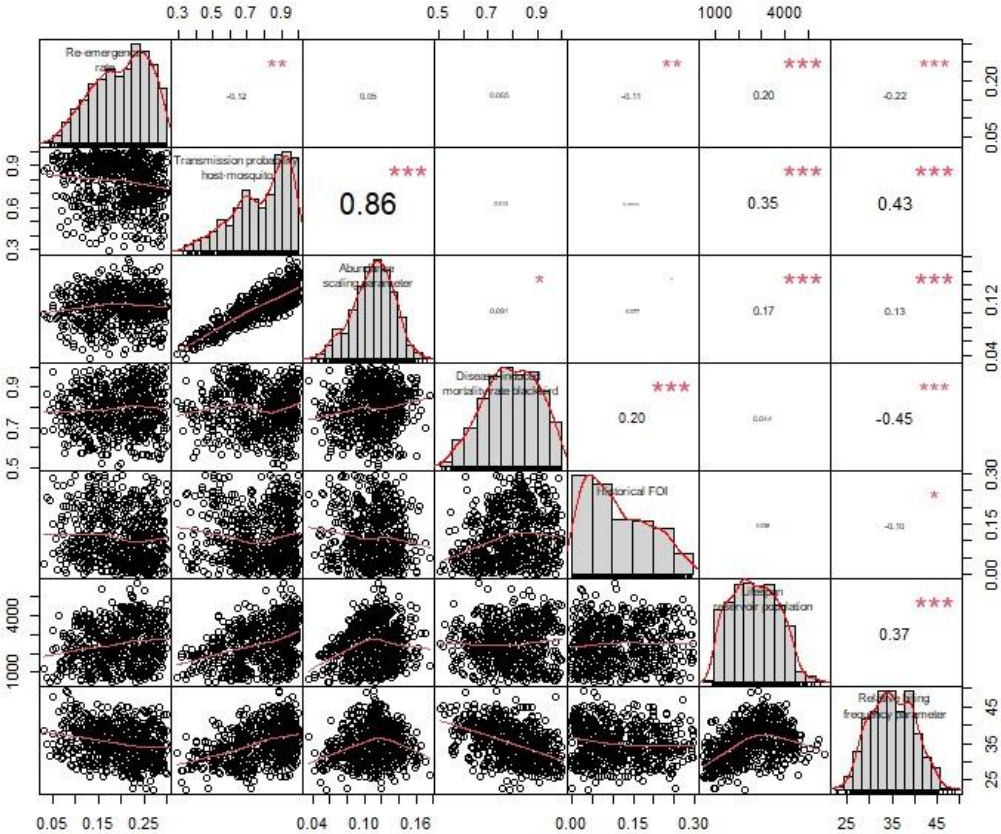

Supplementary figure 29: Correlation plot of posterior distributions for model D.

Supplementary Material H: Reproduction numbers

Derivation of reproduction numbers

Reproduction numbers were calculated using the Next Generation Matrix (NGM) approach. The reproduction number was obtained by calculating the dominant eigenvalue of the NGM. The dimensions of the NGM were 5x5 representing the number of species capable of transmitting the infection (mosquitoes (M), juvenile blackbirds (J), adult blackbirds (A), juvenile reservoir population (R), adult reservoir population (P)). Each element in the NGM, k_{ij} , represents the expected number of cases of type *i* caused by an individual of type *j*:

$$A = \begin{matrix} 0 & K_{MJ} & K_{MA} & K_{MR} & K_{MP} \\ K_{JM} & 0 & 0 & 0 & 0 \\ K_{AM} & 0 & 0 & 0 & 0 \\ K_{RM} & 0 & 0 & 0 & 0 \\ K_{PM} & 0 & 0 & 0 & 0 \end{matrix}$$

All mosquito-to-mosquito and bird-to-bird elements in the NGM are set to zero as transmission only occurred between mosquitoes and birds and vice versa. The value of each of the elements in the NGM was derived as follows:

K_{JM}: The number of infected juvenile blackbirds caused by an infectious mosquito is determined by

- The fraction of mosquitoes transitioning from E to I
- The duration of infectiousness in mosquitoes
- The mosquito-to-juvenile blackbird transmission rate

$$K_{JM} = \frac{u}{(u + \mu_M + \sigma)} * \frac{1}{(\mu_M + \sigma)} * b * q * p_{BM} * \frac{N_J}{((N_R + N_P) * \omega + N_J + N_A)}$$

K_{AM}: The number of infected adult blackbirds caused by an infectious mosquito is determined by

- The fraction of mosquitoes transitioning from E to I
- The duration of infectiousness in mosquitoes
- The mosquito-to-adult blackbird transmission rate

$$K_{AM} = \frac{u}{(u + \mu_M + \sigma)} * \frac{1}{(\mu_M + \sigma)} * b * q * p_{BM} * \frac{N_A}{((N_R + N_P) * \omega + N_J + N_A)}$$

K_{RM}: The number of infected juvenile reservoir hosts caused by an infectious mosquito is determined by

- The fraction of mosquitoes transitioning from E to I
- The duration of infectiousness in mosquitoes
- The mosquito-to-juvenile reservoir transmission rate

$$K_{RM} = \frac{u}{(u + \mu_M + \sigma)} * \frac{1}{(\mu_M + \sigma)} * b * q * p_{BM} * \frac{N_R * \omega}{((N_R + N_P) * \omega + N_J + N_A)}$$

K_{PM}: The number of infected adult reservoir hosts caused by an infectious mosquito is determined by

- The fraction of mosquitoes transitioning from E to I
- The duration of infectiousness in mosquitoes
- The mosquito-to-adult reservoir transmission rate

$$K_{RM} = \frac{u}{(u + \mu_M + \sigma)} * \frac{1}{(\mu_M + \sigma)} * b * q * p_{BM} * \frac{N_P * \omega}{((N_R + N_P) * \omega + N_J + N_A)}$$

K_{MJ}: The number of infected mosquitoes caused by an infectious juvenile blackbird is determined by

- The fraction of juvenile blackbirds transitioning from E to I
- The duration of infectiousness in juvenile blackbirds
- The juvenile blackbird-to-mosquito transmission rate

$$K_{MJ} = \frac{\varepsilon}{(\varepsilon + \mu_J)} * \frac{1}{(\mu_J + \gamma + \nu)} * b * q * p_{MB} * \frac{N_J}{((N_R + N_P) * \omega + N_J + N_A)} * \frac{N_M}{N_J}$$

K_{MA}: The number of infected mosquitoes caused by an infectious adult blackbird is determined by

- The fraction of adult blackbirds transitioning from E to I
- The duration of infectiousness in adults
- The adult blackbird-to-mosquito transmission rate

$$K_{MA} = \frac{\varepsilon}{(\varepsilon + \mu_A)} * \frac{1}{(\mu_A + \gamma + \nu)} * b * q * p_{MB} * \frac{N_A}{((N_R + N_P) * \omega + N_J + N_A)} * \frac{N_M}{N_A}$$

K_{MR}: The number of infected mosquitoes caused by an infectious juvenile reservoir host is determined by

- The fraction of juvenile reservoir birds transitioning from E to I
- The duration of infectiousness in juvenile reservoir birds
- The juvenile reservoir-to-mosquito transmission rate

$$K_{MR} = \frac{\varepsilon}{(\varepsilon + \mu_R)} * \frac{1}{(\mu_R + \gamma)} * b * q * p_{MB} * \frac{N_R * \omega}{((N_R + N_P) * \omega + N_J + N_A)} * \frac{N_M}{N_R}$$

K_{MP}: The number of infected mosquitoes caused by an infectious adult reservoir host is determined by

- The fraction of adult reservoir birds transitioning from E to I
- The duration of infectiousness in adult reservoir birds
- The adult reservoir-to-mosquito transmission rate

$$K_{MP} = \frac{\varepsilon}{(\varepsilon + \mu_P)} * \frac{1}{(\mu_P + \gamma)} * b * q * p_{MB} * \frac{N_P * \omega}{((N_R + N_P) * \omega + N_J + N_A)} * \frac{N_M}{N_P}$$

The elements in the NGM represent partial reproduction numbers, i.e. the reproduction number for a specific transmission route. The effective reproduction number was calculated by multiplying each of the partial reproduction numbers by the proportion of the population that is susceptible to infection. The effective reproduction number was therefore the dominant eigenvalue of the following matrix:

$$A = \begin{matrix} 0 & K_{MJ} * prop.S_M & K_{MA} * prop.S_M & K_{MR} * prop.S_M & K_{MP} * prop.S_M \\ K_{JM} * prop.S_J & 0 & 0 & 0 & 0 \\ K_{AM} * prop.S_A & 0 & 0 & 0 & 0 \\ K_{RM} * prop.S_R & 0 & 0 & 0 & 0 \\ K_{PM} * prop.S_P & 0 & 0 & 0 & 0 \end{matrix}$$

Results related to reproduction number

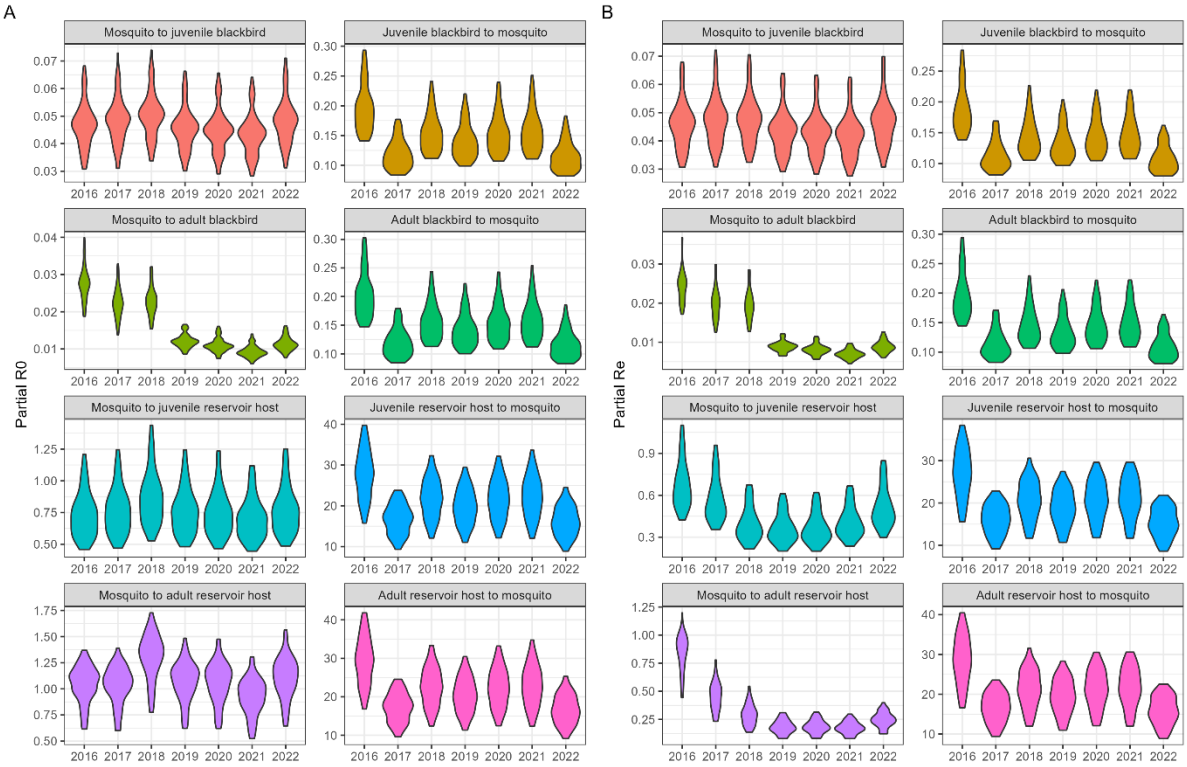

Supplementary figure 30: Annual partial reproduction numbers (basic (A) and effective (B)) during transmission season from April to October.

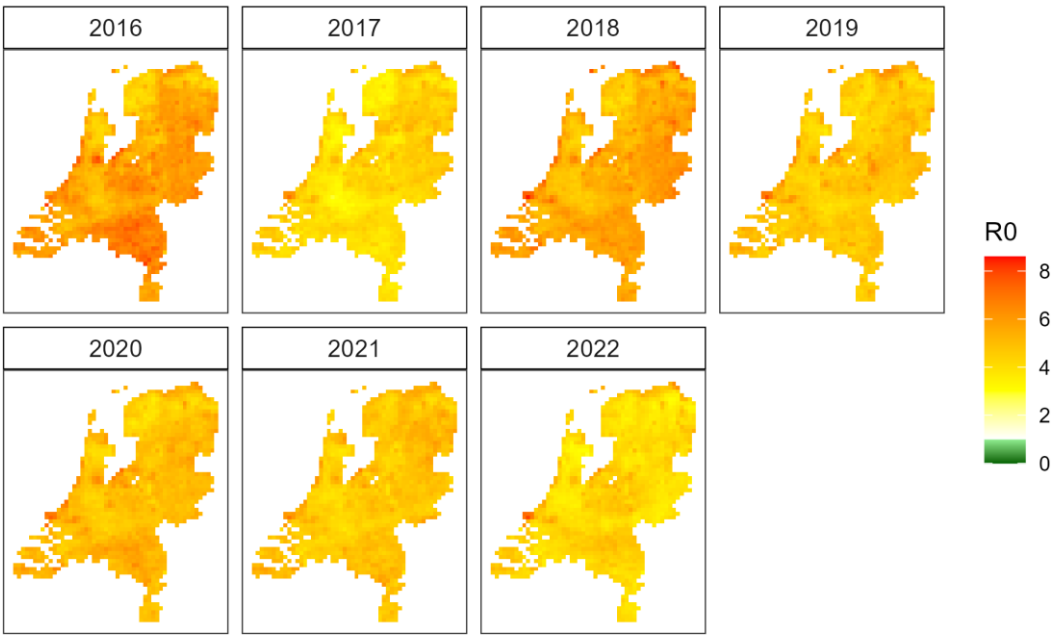

Supplementary figure 31: Map of mean basic reproduction number during the transmission season (April to October)

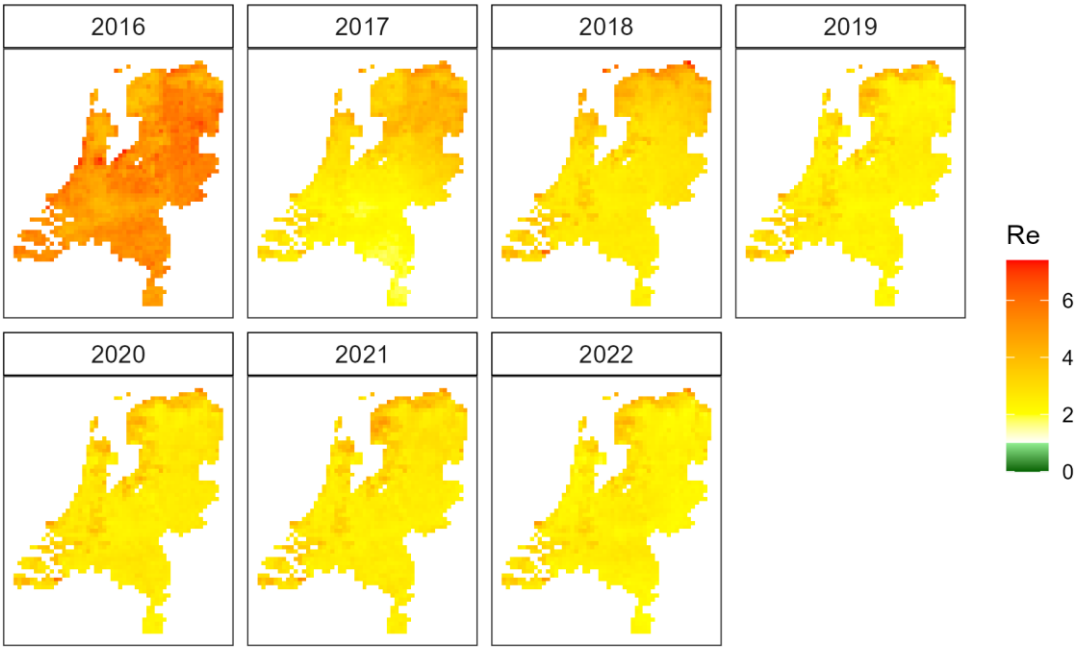

Supplementary figure 32: Map of mean effective reproduction number during the transmission season (April to October)